Studying meiosis in mitosis: Activating the meiosis-specific Red1-Hop1-Mek1 complex in mitotic budding yeast cells

Vaishnavi N. Nivsarkar[1,2] Linda Chen [6], Saskia K. Funk [6], John R. Weir [6] and Gerben Vader [1,3,4,5,*]

[1] Department of Mechanistic Cell Biology, Max Planck Institute of Molecular Physiology, Otto-Hahn-Strasse 11, 44227, Dortmund, Germany

[2] IMPRS for Living Matter, Max Planck Institute of Molecular Physiology, Otto-Hahn-Strasse 11, 44227, Dortmund, Germany

[3] Amsterdam UMC location Vrije Universiteit, Section Oncogenetics, Department of Human Genetics, De Boelelaan 1118, Amsterdam, The Netherlands

[4] Cancer Center Amsterdam, Cancer Biology and Immunology, Amsterdam, The Netherlands

[5] Amsterdam Reproduction & Development, Amsterdam, The Netherlands

[6] Structural Biochemistry of Meiosis Group, Friedrich Miescher Laboratory, Max-Planck-Ring 9, 72072 Tübingen, Germany

[*] to whom correspondence should be addressed: g.vader@amsterdamumc.nl

ORCID: 0000-0002-4876-1234 (VNN)
0000-0003-2136-2142 (LC)
0000-0002-6904-0284 (JRW)
0000-0001-5729-0991 (GV)

Abstract

In mitosis, sequences on sister chromatids are preferred as DNA repair templates, whereas in meiosis interhomolog-based repair is promoted. The switch of template preference during homologous recombinational (HR) repair of DNA breaks is a defining event in sexual reproduction. This preference is needed to establish linkages between homologous chromosomes that support meiotic chromosome segregation. In budding yeast, a central activity that enforces meiotic interhomolog bias is encoded in a meiosis-specific protein kinase complex, consisting of Red1, Hop1 and Mek1 (*i.e.,* the RHM complex). Activation of Mek1 kinase in meiosis – dictated by complex formation and upstream DNA break-dependent signaling – leads to modification of HR factors and the establishment of interhomolog HR repair bias. How meiotic repair bias is established is a central question with implications for sexual reproduction, genetic diversity and genome stability. Studying the role of the RHM complex in DNA repair is complicated by the fact that Red1 and Hop1 are required for efficient meiotic DNA break formation. Here, we conditionally express RHM components in mitotically-dividing cells to show that these factors can autonomously establish the RHM complex outside of its physiological environment. *In vivo* analysis is complemented with *in vitro* biochemical reconstitution to analyze the composition of a Red1-Hop1 subcomplex. The RHM complex can be activated under DNA damaging conditions in mitotically-dividing cells, and activation depends on upstream Mec1 kinase function. We use this system to perform a structure-function analysis of RHM complex formation and Mek1 activation. Finally, we demonstrate that expressing active Mek1 in mitosis leads to *rad51Δ*-like DNA break sensitivity, suggesting that activation of the RHM complex is sufficient to reconstitute (parts of) its physiological function in mediating HR-based repair. This system should enable querying downstream effects of RHM complex action on DNA repair dynamics and template bias. Human homologs of Red1 and Hop1 are often aberrantly re-expressed in cancer cells. Our system has the potential to inform on (dys)functional effects of these genes on genome stability during human tumorigenesis.

Introduction

Eukaryotes rely on meiosis to produce reproductive cells (*i.e.*, sperm, egg or spores) that enable sexual reproduction. The biochemical principles that drive meiosis are similar to the canonical mitotic cell cycle, with additional meiosis-specific processes driving unique events required for gamete production [1]. Meiosis can thus be seen as an adaptation of the mitotic cell cycle. One approach to understand meiosis-specific mechanisms is via reconstitution in non-physiological environments, for example via *in vitro* biochemical reconstitutions (*e.g.*, [2–7]), or by expressing meiosis-specific factors in non-meiotic cells (*e.g.*, [8–12]).

A hallmark of meiosis is a bias during homologous recombination (HR)-based DNA repair to use repair templates present on homologous chromosomes over those on sister chromatids [13]. Such 'interhomolog' (IH) bias promotes repair of programmed DNA double strand breaks (DSBs) into interhomolog crossovers – a prerequisite for chromosome assortment and gamete production. This type of repair constitutes a remarkable adaptation of canonical HR repair in mitotically dividing cells, where sister chromatids are the preferred repair template during HR [14]. In budding yeast, the intersister-to-interhomolog template switch is controlled by the Red1-Hop1-Mek1 complex (*i.e.* the RHM complex) (reviewed in [13]). *RED1*, *HOP1* and *MEK1* are specifically expressed in meiosis, and they function as a discrete complex [6,7,15–18]. Red1 is a filamentous protein that is loaded onto meiotic chromosomes [6,16]. Loss of Red1 *i)* disrupts meiosis-specific axis-loop chromosome organization [19], *ii)* severely impacts (Spo11-dependent) programmed DSB formation, *iii)* causes loss of interhomolog repair bias, and *iv)* leads to spore viability defects [20–23]. Hop1 associates with Red1 via the NH_2-terminal HORMA domain, which can topologically embrace a short peptide motif (termed closure motif; CM) present in Red1 [6,17,18,24] (**Figure 1a**). Hop1 is also a component of the meiotic chromosome axis [25] and required for efficient DSB formation and interhomolog bias during repair [21,24]. In addition to a HORMA domain [26,27], Hop1 contains a COOH-terminal region which is involved in protein-protein interactions. The COOH-terminal end of Hop1 harbors a CM (*i.e.* a HORMA domain-binding peptide), which can be captured by Hop1's HORMA domain [17,26,28], potentially forming Hop1-to-Hop1 beads-on-a-string assemblies [29] or intramolecular CM-HORMA associations [17,29,30]. Red1 and Hop1 are associated with 'chromosome axis' sites defined by meiotic (*i.e.* Rec8-containing) cohesin [31,32]. Rec8-cohesin drives recruitment of Red1 and Hop1, potentially via a direct association [32], although a cohesin-independent pathway that promotes Red1/Hop1 recruitment has also been described [33]. Red1 and Hop1 are involved in recruiting DSB factors to chromosome axis sites, likely via a direct association of DSB factors with Hop1 [7,31,32,34,35]. Mek1, the third component of the RHM complex, is a serine-threonine protein kinase that in addition to its kinase domain, contains a Forkhead-associated (FHA) domain – a phospho-peptide binding domain [36,37]. Mek1 is similar to Rad53, a key DNA damage checkpoint kinase in mitotically-growing cells [38]. Meiotic DSB formation triggers a checkpoint cascade known as the meiotic prophase or pachytene checkpoint [39,40]. Central to this checkpoint are sensor kinases, Tel1 and Mec1 – the budding

yeast homologs of ATM and ATR, respectively – that also respond to mitotic DNA damage [38]. Tel1 is activated at DSB sites, whereas Mec1 activation requires the presence of ssDNA tracts generated around DSB sites, through the action of defined nucleases. ssDNA tracts also serve as intermediates in homologous recombination-based DNA repair. Mec1/Tel1 phosphorylate downstream substrates to coordinate cell cycle arrest with DNA repair. In mitosis, a central downstream kinase in the Mec1/Tel1 cascade is Rad53 (the budding yeast homolog of Chk2). Rad53 activation relies on Mec1/Tel1-dependent phosphorylation of its adaptor protein, Rad9 [41–43]. Normally, Rad53 is not activated in meiosis [44], and its role in the meiotic checkpoint is taken over by Mek1 [45]. Hop1 plays a role that is conceptually similar to Rad9 for Mek1: it is a substrate of Mec1/Tel1, and its phosphorylation leads to chromosomal recruitment and activation of Mek1, likely via induced dimerization of Mek1 [46–49]. Activated Mek1 phosphorylates downstream substrates [37,50–52], eventually leading to cell cycle arrest and DNA repair. as such influencing cell cycle arrest and DNA repair. By impinging on the meiotic transcription factor Ndt80 [50,53], Mek1 halts meiotic cell cycle progression until DSB repair is complete [37]. Furthermore, Mek1 activity promotes the establishment of IH repair bias [54,55]. Mek1 substrates that impact DNA repair outcome have been identified, prominently among them Rad54 [56,57]. Rad54 is an accessory factor to the DNA recombinase Rad51 [58,59], and phosphorylation of Rad54 inhibits the ability of Rad51 to promote homologous recombination [56,57]. A germane question is how an inhibitory effect on Rad51-dependent HR could lead to the promotion of interhomolog-biased repair. A model put forward by Subramanian and Hochwagen posits that this inhibitory effect – when locally restricted by virtue of required vicinity to DSB sites – might specifically prevent repair utilizing template on sister chromatids that reside in vicinity of the DSB (by virtue of sister chromatid cohesion) [60]. Localized DSB repair inhibition could lead to exploration into distant repair template searches beyond the sphere of influence of localized Mek1 activity, eventually resulting in IH-based repair 'activation'.

The formation of crossovers appears to be a near-universal prerequisite for successful gamete formation, but little is known about the molecular regulation of this process outside of budding yeast [13]. Nonetheless, functional homologs of the non-enzymatic subunits of the RHM complex (Red1 and Hop1) can be recognized outside of budding yeast [61]. It is thus a distinct possibility that a complex that is functionally and molecularly analogous to the budding yeast RHM complex (possibly with Chk2 kinase as enzymatic component [62]) plays a conserved role in establishing unique DNA repair dynamics, also during human sexual reproduction.

In this study, we present the development of an experimental system that allows for the controlled formation and activation of the meiosis-specific RHM complex in mitotically-dividing budding yeast cells. This system creates new possibilities to study the molecular details underlying the establishment of meiosis-specific DNA repair.

Material and Methods

Yeast strain construction and genetics

Budding yeast (*Saccharomyces cerevisiae*) strains were of the W303 or SK1 background. Genotypes of the used strains are listed in **Supplementary Table 1**. For construction of galactose-inducible expression alleles, *pGAL1*, *pGAL1::GFP, pGAL1::GST* or *pGAL1::3HA* constructs were integrated directly upstream of the start codons of *HOP1*, *MEK1* or *RED1* using PCR-based gene targeting [63]. *RED1* NH_2-terminal truncations were generated by integration of *pGAL1::3HA* at desired codon sites. COOH-terminal truncations were made by introduction of a STOP codon (via integration of a *TRP1* marker including a STOP codon [63]) in a *KANMX6::pGAL1::3HA-RED1* containing strain. Integration of constructs was confirmed by PCR. Subsequent strains were generated by yeast genetics and tetrad dissection.

Growth conditions, galactose-based expression induction and drug treatments

Strains were grown on YP-glycerol plates, transferred to YP-glucose (YPD) plates and grown overnight. Cultures were grown in YP-raffinose/glucose (YPRG) media (2.4% Raffinose, 0.12% Glucose) overnight at 30°C till saturation. In the morning, cultures were diluted to a final OD_{600} of 0.48 and further grown for 3.5 hours in YP-RG before adding 2% Galactose. Samples were collected at indicated time points. See **Supplementary Figure 1** for schemes depicting various treatment regimens. For DNA damage drug treatment, 0.01% (v/v) methyl methanesulfonate (MMS, Sigma-Aldrich) was added 30 minutes prior to galactose induction. Alternatively, phleomycin (Sigma-Aldrich) treatment was performed by adding 50 μg/ml (30 minutes prior to galactose addition). Phleomycin was re-added 2 hours after galactose-based induction. For enrichment of cells in G1, secondary cultures were grown for 2.5 hours followed by the addition of α-factor (166 μg/ml; home-made). A second dose of α-factor (50 μg/ml) was added after 1 hour of galactose induction. For nocodazole-induced G2/M arrest, secondary cultures were treated with nocodazole (15 μg/ml; Sigma-Aldrich) 3 hours after starting secondary cultures. Nocodazole (15 μg/ml) was re-added 3 hours after adding galactose. For meiotic time courses (Figure 1D and 3b), cells were treated and cultured as described in detail in [64].

Yeast viability assays

Cells were inoculated into liquid YP-RG media overnight at 30°C. The next day, cells were diluted to OD_{600} 1 in H_2O. 5 µl of 10-fold dilutions were spotted on YP-glucose or YP-galactose plates. Growth at 30°C was monitored for the following 2–4 days.

Cell cycle analysis

Flow cytometry was used to monitor cell cycle status. Briefly, 150 μL of yeast cultures were fixed (2 hours at 4 ºC) in 70% EtOH. Fixed cells were pelleted and incubated overnight at 50 ºC in 500 μL Sodium Citrate (50 mM) with 0.7 mL RNase A (30 mg/ml; Sigma-Aldrich). Cell suspensions were treated with proteinase K (20 mg/ml; VWR) for 2 hours at 50 ºC. DNA was stained by addition of 500 μL of Sodium Citrate (50 mM) containing 0.2 μL SYTOX-Green (Life Technologies). Cells were disrupted by brief sonication, and DNA content was measured using a BD AccuriTM C6 (BD Biosciences) flow cytometer. Samples were taken at the indicated time points, and 10,000 events were counted. Data was analyzed using FlowJo (FlowJo LLC).

SDS-PAGE and western blotting

Samples were harvested at indicated time points by harvesting the equivalent of 5 ml OD_{600} 1.9 from the cultures. Cell pellets were precipitated with 5 ml 5% TCA and washed with acetone. Pellets were dried overnight, and were resuspended in 200 ml of protein breakage buffer (10mM Tris (pH 7.5), 1 mM EDTA, 2.75 mM DTT). ~0.3g of acid-washed glass beads was added, and cell breakage was performed by using a FastPrep-24 (MP Biomedicals). Samples were diluted by adding 100 µl of protein breakage buffer and 150 µl of 3x SDS loading buffer. To observe histone modifications, 15% SDS-PAGE gels were used. 15% Gels were run at 70 Volt for 100 minutes. Protein transfer was done on PVDF membranes (phospho-histone detection) or on nitrocellulose membranes (other proteins). Primary antibodies were used as follows: α-HA (Biolegend 901502; 1:500), α-Pgk1 (Thermo Fisher; 1:1000), α-GFP (home-made; 1:5000), α-Hop1 (home-made; 1:10,000, see [65]), α-phospho-Histone H3-Threonine 11 (EMD Millipore 05-789, 1:1500), and α- phospho-Histone H2A-Serine 129 (Abcam 181447, 1:500 in 4% BSA/TBS-Tween). All antibody incubations were in 5% milk/PBS-Tween, unless stated otherwise.

Co-immunoprecipitation

Secondary cultures were grown for 3.5 hours followed by 2% galactose addition for 4 hrs. The equivalent of 50 ml of cultures (OD_{600} 1.9) were spun down at 3000 rpm for 3 minutes. Samples were washed with cold H_2O and snap frozen. 300 µl of ice-cold IP buffer (50 mM Tris–HCl pH 7.5/150 mM NaCl/1% Triton X-100/1 mM EDTA pH 8.0, with a cocktail of protease inhibitors freshly added) and acid-washed glass beads were added. Cells were broken in a FastPrep-24 disruptor (MP Biomedicals) by two 50-s cycles (speed 6). Cell lysate was spun 30 seconds at 500 rpm, and the supernatant was transferred to a 15 mL falcon tube, followed by sonication for 25 cycles (30 seconds on/30 seconds off, high power range) on a Bioruptor-Plus sonication device (Diagenode), and spun down 30 minutes at maximum speed. Supernatant (total of 500 µl) was transferred to a new microcentrifuge tube, and 10% of the supernatant (50 µl) was collected as input. For α-HA IPs, 1 µl of antibody (α-HA; BioLegend) was added to the lysate and rotated for 3 h. Lysates were incubated with 30 µl of Dynabeads protein G

(Invitrogen, Thermo Fisher Scientific) overnight at 4°C. For α-GFP-based IPs, 1 µl α-GFP (home-made) were used, in combination with 30 µl of Dynabeads protein G. After incubation, beads were washed four times with 500 µl of ice-cold IP buffer. For the final wash, beads were transferred to a new microcentrifuge tube and resuspended in 40 µl IP buffer. 20 µl of SDS-loading buffer was added to samples and samples were incubated for 5 minutes at 95° C. Inputs were treated as follows: supernatant was precipitated with 10% TCA (*i.e.* 5 µl), and samples were incubated on ice for 30 minutes. Pellets were collected by centrifugation (1 minute at maximum speed), and washed with ice-cold acetone. After centrifugation and removal of supernatant, precipitations were dried on ice, resuspended in TCA-resuspension buffer (50 mM Tris–HCl 7.5/6 M urea), and incubated on ice for 30 minutes. Precipitates were dissolved by careful pipetting and vortexing. 10 µl of SDS-loading buffer was added, and samples were incubated for 5 minutes at 95°C. IP and input samples were analyzed by SDS-PAGE followed by western blotting.

Cloning and purification of the Hop1-Red1 complex

DNA sequences corresponding to Hop1 (Uniprot ID P20050) and Red1 (Uniprot ID P14291) were amplified from yeast genomic DNA (SK1 strain), and cloned into vectors from the InteBac suite [66]. Hop1 was cloned with a 3C cleavable N-terminal 2xStrep-II tag for insect cell expression (plasmid ID pWL661), and Red1 with a C-terminal MBP fusion, also for insect cell expression (plasmids ID pWL1157). Expression plasmids were used to generate bacmids via the EMBacY cell line [67]. Bacmids were used to transfect SF9 cells using FuGene HD (Promega). Baculovirus was generated through three rounds of amplification in SF9 cells grown in Sf-900 III media (ThermoFisher). For expression of the Hop1-Red1 complex, Hi5 cells were infected at a 1:100 (v/v ratio) amplified virus of both pWL661 and pWL1157 and the cells were cultured for 72 hours post infection. Cells were harvested, washed once in PBS and resuspended in lysis buffer (50 mM Na-HEPES pH 7.5, 300 mM NaCl, 10% Glycerol, 1 mM $MgCl_2$ 10 μM $ZnSO_4$) the buffer was also supplemented with both cOmplete EDTA-free protease inhibitor (Roche) and Benzonase (Merck). Cells were lysed by sonication, cleared by ultracentrifugation, and passed over a Streptactin-XT column (IBA Lifesciences). Samples were eluted in lysis buffer supplemented with 50 mM biotin. Sample purity was analysed on SDS-PAGE stained with Coomassie Brilliant Blue.

Mass Photometry

A RefeynOne Massphotometer (Refeyn Ltd., Oxford UK) was used to determine the molecular mass of samples in solution. Samples of Hop1-Red1 were diluted in lysis buffer to ~30 nM prior to measurement. Molecular mass was determined in Analysis software provided by the manufacturer using a NativeMark (Invitrogen) based standard curve created under the identical buffer composition.

Cross-linking Mass Spectrometry

For XL-MS analysis proteins were dissolved in 200 ul of 30 mM HEPES pH 7.5, 1 mM TCEP, 300 mM NaCl to final concentration of 3 μM, mixed with 3 μl of DSBU (200 mM) and incubated for 1 hour in 25 °C. The reaction was quenched by addition of 20 μl of Tris pH 8.0 (1 M) and incubated for another 30 min in 25 °C. The crosslinked sample was precipitated by addition of 4X volumes of 100% cold acetone ON in -20 °C and subsequently analyzed as previously described [68].

AlphaFold2

We made use of the CoLabFold implementation of AlphaFold [69,70], using mmseqs2 instead of Jackhammer to produce the MSA. We generated five models using 3 recycles and one ensemble per model. The models were ranked based on pLDDT score. We used the top-ranked model for our analyses, which gave an overall pLDDT score of 67.25.

Results

We established a system to express subunits of the meiosis-specific Red1-Hop1-Mek1 (RHM) complex in non-meiotic budding yeast cells (**Figure 1a**). We placed the galactose-responsive *pGAL1* promoter in front of the coding regions of the genes encoding Red1, Hop1 and Mek1 – note that in case of *RED1* and *MEK1*, we added NH_2-terminal affinity tags (3HA and GFP, respectively) to enable antibody-based detection (**Figure 1b**). When grown under conditions that lacked galactose, cells did not express *RED1*, *HOP1* or *MEK1*, and galactose addition led to rapid expression (**Figure 1c**). Protein levels of Hop1 upon mitotic *pGAL1*-driven expression were compared with endogenous protein levels (*i.e.,* in meiotic prophase cells, when RHM complex subunits are expressed and functional) (**Figure 1d**). 2 hours of galactose-driven induction yielded Hop1 levels that were comparable with meiotic prophase protein levels. The levels of Hop1 in mitotically-dividing cells increased further upon longer induction (*i.e.,* after 4 hours). Thus – at least in the case of Hop1 – mitotic protein levels are comparable to those seen under physiological conditions in meiosis. We generated strains expressing different combinations of the three *pGAL1*-regulated genes, and confirmed co-expression of *RED1*, *HOP1* and *MEK1* (**Figure 1e**). Under certain combinations we observed effects on protein stability – for example, Mek1 protein levels were consistently elevated when Hop1 and Red1 were also co-expressed, as compared to conditions where Mek1 was expressed in isolation (*e.g.,* compare α-GFP (Mek1) signal in lane 2 and 14 of **Figure 1e**). This could be a reflection of protein stabilization brought about by the presence of cognate binding partners, such as components of a defined protein complex as in the case of the RHM complex. This observation thus hints at the possibility that Red1, Hop1 and Mek1 might associate under these conditions.

The galactose-controllable strains allowed us to investigate the behavior of mitotic yeast cells under conditions where this meiosis-specific complex (or a combination of its subunits) is expressed. We tested whether expression of these three meiotic factors (individually or in combinations) affected mitotic cell growth. We plated serial dilutions of strains that harbor different combinations of *pGAL1*-driven *RED1*, *HOP1* and *MEK1* on glucose or galactose containing plates and monitored growth (**Figure 1f**). Cells expressing *RED1* experienced a growth defect, whereas no observable growth effects were seen in cells that expressed *HOP1* or *MEK1* in isolation. Expressing different combinations of the RHM complex revealed that the growth defect observed in *RED1*-expressing cells was aggravated by co-expression of *HOP1* or *MEK1*, and was severely increased when all three factors were expressed simultaneously (**Figure 1f**). No defects were observed in cells co-expressing *HOP1* and *MEK1* in the absence of *RED1*. To address whether the observed growth defects were associated with specific mitotic cell cycle delays, we monitored DNA content using flow cytometry. *RED1* expression caused an increase in cells that contained a 2N DNA content, indicating a delay/arrest in G2 or mitosis (**Figure 1g**). These results are in line with a systematic survey of overexpression on mitotic yeast cells [71], which reported effects of *RED1* overexpression on cell cycle progression. *RED1*-dependent effects were

exacerbated by co-expression of *HOP1* and *MEK1* (**Figure 1f**), mirroring the general growth defects presented in **Figure 1g**. Thus, the presence of Red1 is poorly tolerated by mitotic cells, and that this effect is exacerbated when Hop1 and/or Mek1 are also present. Red1 can form higher-order assemblies – specifically tetramers – as well as filaments of tetramers [6,15,24]. Effects on cell growth might be related to this characteristic of Red1 (see also below).

We tested whether these factors could associate to form a trimeric complex, as in meiosis. Immunoprecipitation of Red1 led to the specific enrichment of Mek1 or Hop1, demonstrating that Red1 is able to establish an interaction with either of these factors in mitotic cells (**Figure 2a**). A similar enrichment between RHM components was observed upon co-immunoprecipitation of GFP-Mek1 (**Figure 2b**). Co-expression of *HOP1* and *MEK1* with *RED1* led to enrichment of Hop1 as well as Mek1, suggesting that under these conditions, a RHM complex can be established. As such, these data suggest that RHM complex formation can be accomplished when expressed outside of its normal physiological condition in yeast cells. The RHM complex can thus autonomously be established in mitotic cells without the need for meiosis-specific factors or modifications. These data suggest also that, in addition to its described interaction with Hop1 (via its CM, encoded in $Red1_{340-362}$; see also below [6,18,24]), Red1 appears to encode a Mek1-interaction region. Red1 contains a conserved structured NH_2-terminal domain (amino acids 1-340) – likely encoding an Armadillo repeat (ARML) domain and a Pleckstrin homology (PH) domain [61,72,73] (**Figure 2c,** and see below). This module is followed by a CM sequence ($Red1_{340-362}$) that mediates interaction with Hop1 [17,24]. This region is followed by a large (predicted to be unstructured) region ($Red1_{340-362}$) and a COOH-terminal coiled-coil region ($Red1_{340-362}$) [6,15,24]. This coiled-coil domain of Red1 harbors tetramerization as well as filament forming activities [6,15]. Filamentous Red1 assemblies are thought to be crucial to establish the meiotic chromosome structure [6,15]. Mutations that disrupt this filamenting domain lead to defects in meiotic chromosome organizations and spore viability [74,75]. Truncation of the extreme COOH-terminal region of Red1 (*i.e.* removal of the last 7 amino acids) was shown to lead to a specific disruption of filament formation, while leaving tetramerization unaffected [6,15]. We generated a series of alleles of Red1 (all driven by *pGAL-3HA*), based on these established structural features of Red1 (**Figure 2c**). We performed co-immunoprecipitation analysis to investigate the requirement of Red1 to interact with Hop1 and/or Mek1, the result of which are presented in Figure 2D and E. We initially focused on the well-defined interaction between Red1 and Hop1. We found that, as in meiosis, the interaction between Hop1 and Red1 depended on the presence of the CM within Red1 ($Red1_{340-362}$) [17,24]. A construct of a Red1 expressing the first 345 amino acids but lacking the CM failed to co-purify Hop1 ($Red1_{1-345}$; **Figure 2d**). Second, a Red1 fragment that included the key residues in the CM of Red1 ($Red1_{346-827}$) was able to interact with Hop1, whereas a progressively larger truncation which removes the CM of Red1 ($Red1_{346-827}$) failed to bind to Hop1. Full length Red1 (thus also encoding the structured ARM/PH module directly adjacent to the CM) appeared to bind more efficiently to Hop1 as compared to the

version of Red1 that was truncated upstream of the CM (**Figure 2e**). The domain organization of Red1, in which the CM is located immediately adjacent to a structured region, might thus influence Hop1-Red1 association. The structured NH_2-terminal domain might prevent 'sliding off'-based dissociation of CM in Red1 from the HORMA domain of Hop1, similar to what was recently described for the association between the HORMA domain of Mad2 and its topological binding partner Cdc20 [76]. Alternatively, the NH_2-terminal of Red1 directly upstream of the CM could ostensibly also contribute to Hop1 binding more directly via the establishment of interactions with Hop1. We next focused on the association of Mek1 with Red1 and Hop1. A fragment of Red1 that contains its NH_2-terminal structured domain ($Red1_{1-345}$) was able to pulldown Mek1 (**Figure 2d**), whereas truncated Red1 fragments that lacked this domain but contained the COOH-terminal part of Red1 (*e.g.,* $Red1_{346-827}$ or $Red1_{367-827}$) were also proficient for Mek1 interaction (**Figure 2e**). Both associations occurred under conditions where Hop1 was not present within the complex (see pulldowns for $Red1_{1-345}$ and $Red1_{367-827}$ in **Figure 2d and e**), suggesting that these Red1-Mek1 associations can be established in the absence of Hop1. Thus, at least under our mitotic expression conditions, Red1 contains two (apparently independent) binding sites for Mek1. We correlated our Red1 truncation-interaction analysis with our earlier findings that expression of full length Red1 (in isolation, or in combination with Hop1 and/or Mek1) led to growth defects (**Figure 1f and g**). We expressed different Red1 constructs, and queried effects on cell growth. Expression of Red1 fragments that contained the extreme COOH-terminal amino acid stretch known to lead to filament/tetramer formation led to cell growth that were comparable to those seen upon the expression of full length Red1 (**Figure 2f**). Removing the filament-forming amino stretch abrogated these effects [6,15], hinting that the observed phenotypes on cell cycle progression and growth are linked to Red1 filament formation.

In order to gain additional insight into the interaction between Hop1 and Red1, we analyzed this complex using *in vitro* analysis of purified components. We succeeded in purifying a complex of NH-terminally 2xStrepII-tagged Hop1 with COOH-terminally MBP-tagged Red1, via Streptactin-based affinity purification from insect cells (**Figure 3a**). To enable expression and purification, we mutated Red1 in the COOH-terminal coiled-coil region ($Red1_{I743R}$) to prevent the formation of filaments, as previously described [6]. To determine the mass of our assembly in solution, we analyzed our purified complex using mass photometry (**Figure 3b**). The largest species we observed was determined at ~209 kDa, which corresponds well to a 1:1 complex of Hop1 and $Red1_{I743R}$ (theoretical molecular mass of 212 kDa). We observed no species that would correspond to a Red1 tetramer, and we assume this to be a concentration dependent effect, consistent with other components of the synaptonemal complex [4,77], to which the C-terminus of Red1 is functionally and evolutionarily related [73]. We also observed masses that correspond to both free Hop1 and free $Red1_{I743R}$-MBP (~81 kDa and ~140 kDa respectively; theoretical mass 71 kDa and 138 kDa, respectively). As such, we conclude that a 1:1 Hop1-$Red1_{I743R}$ complex can form *in vitro*, but that this complex has partly dissociated at the low concentration (30 nM)

of complex employed for mass photometry. We note that we also have an excess of Hop1 in our preparations, as can be seen in **Figure 3a**. We subjected the Hop1-Red1$_{I743R}$ complex to cross-linking with the bifunctional cross-linker DSBU, followed by proteolytic digestion and mass spectrometry, as described in [68] (**Figure 3c**). Analysis of obtained cross-links revealed that Hop1 appears to be more extensively cross-linked than Red1$_{I743R}$-MBP, possibly reflecting excess free Hop1 in our purification (**Figure 3a** and **b**). In Red1$_{I743R}$-MBP, we observed a single long-distance cross-link between the C-terminal coiled-coil domain and the ARM/PH domain, which could conceivably either be an inter- or intramolecular crosslink. Based on the previously described mode of interaction between Hop1 and Red1, we would expect extensive cross-links between the HORMA domain of Hop1 and a region proximal to the CM of Red1 [17,24]. We indeed observed several cross-links that were consistent with such an interaction (**Figure 3c**). In addition, we also detected extensive cross-links between the NH_2-terminal ARML-PH domain of Red1 and Hop1 (**Figure 3c**; green and red lines). We made use of the recently described AlphaFold2 prediction algorithm [70] to make a predicted model of the Hop1-Red1$_{I743R}$ complex, and to incorporate our crosslink dataset (**Figure 3d** and **Supplementary Figure 2a**). Due to the current limitation of the algorithm, we did not use the full-length Red1 sequence, but rather the first 500 amino acids of Red1 (including the NH_2-terminal domain and the CM; Red1$_{1-500}$), together with full-length Hop1. We carried out 5 iterations of the AF2 algorithm and chose the highest ranked model (based on pLDDT score) for further analysis. The first 345 residues of Red1 fold into two distinct domains, one from 1-230, and a second between residues 231-344. A DALI search [70,78] revealed that, as expected, the full NH_2-terminal globular domain of Red1 (residues 1-345) is overall most similar to the crystal structure of NH_2-terminal domain of SYCP2, with a C_α RMSD of 3.9Å [72]. DALI searches with both the first and second NH_2-terminal domains of Red1 separately showed that the N-terminal half of the NH_2-terminal domain (residues 1-226) corresponds to an armadillo-like repeat domain (ARML), as reported [61,72,73]. The second part of the NH_2-terminal domain (residues 227-345) is indeed predicted to form a PH domain, as suggested [61,72,73,79], with similarity to the PH domain found in the Spo11-associated protein REC114 [80]. Intriguingly, also in light of the participation of Mek1 kinase into the RHM complex and apparent direct association between Red1 and Mek1 (**Figure 2d**), the first NH_2-terminal domain (*i.e.,* the ARML domain) is modelled to be structurally most similar to MO25β (PDB 3ZHP [81] with a C_α RMSD of 2.9 Å (over 152 residues), **Supplementary Figure 3a-d**). MO25β is an kinase adapter protein that enables kinase activation [81]. We used the structure of the STK24 kinase with MO25β [81] to superimpose Mek1 onto the STK24 kinase (C_α RMSD of 2.6 Å (over 233 residues)), **Supplementary Figure 3c**). Based on this model, we suggest that the ARML domain region in Red1 might possibly be involved in interaction (and activation) of Mek1. Sequence conservation mapping onto the surface of the Red1 ARML domain reveals that the region predicted to be in contact with Mek1 kinase is highly conserved (**Supplementary Figure 4a-b**). Strikingly however, in our prediction, the potential kinase binding site present in this region of Red1 is occupied by the rest of NH_2-terminal

domain of Red1 (PH domain, residues 227-345) (**Supplementary Figure 3a-d**). This suggests a potential allosteric regulation of the Mek1-Red1 interaction and activation, whereby the position of the PH domain relative to the AMRL domain might influence Mek1 association. Structure prediction of Hop1 reveals both the expected NH_2-terminal HORMA domain (residues 16-319), but also a second folded domain (residues 328-533) around the region that was previously reported to be a zinc finger [79]. A DALI search of this domain suggests it to be a combination of a winged-helix and PHD domain, as suggested [61,79]. The model placed the CM of Red1 in the HORMA domain of Hop1, as expected (**Figure 3d**, indicated)[17]. In our model, the NH_2-terminal domain of Red1 showed close proximity to the HORMA domain of Hop1, suggesting a potential contribution of this domain to Hop1 binding (**Figure 3d** and **Supplementary Figure 3e**). In an attempt to validate this AF2 prediction of Hop1-Red1$_{1\text{-}500}$, we modelled intersubunit crosslinks onto the obtained model (**Figure 3d**). Based on the length of the used crosslinking agent, we considered crosslinks that are between C_α's within a distance of 40 Å of one another within the model to be consistent with the model (**Figure 3d**, green lines), and those further apart to be inconsistent (**Figure 3d**, red lines)[68]. 11 of the 16 inter-chain cross-links between Hop1 and Red1$_{1\text{-}500}$ are consistent with our established model (**Figure 3e**). Consistent with the data derived from our crosslinking analysis, the model showed a high degree of confidence in folding of the HORMA and PHD domains of Hop1, and especially in the NH_2-terminal domain of Red1 relative to the HORMA domain of Hop1 (**Supplementary Figure 2a**). The algorithm reported a good level of confidence in the placement of the NH_2 terminal domain or Red1 relative to the HORMA domain of Hop1 (**Supplementary Figure 2b**). Additional attempts to model full-length Hop1 with Red1 1-500 showed the placement of the PHD domain relative to the other domains of the complex was reported to have low confidence (data not shown). Our analyses shed light on the establishment of the Red1-Hop1 complex (and by extension likely provide insight into assembly of the entire RHM complex). Our *in vitro* data (**Figure 3**) are consistent with our *in vivo* data (**Figure 2e**): both sets of data suggest that the NH_2-terminal domain of Red1 (and specifically the ARML) might contribute directly to the association between Red1 and Hop1.

A central functionality of the RHM complex in mediating DNA repair template decisions (and checkpoint function) lies in the kinase activity of Mek1, which leads to defined downstream phosphorylation events [50–52,82]. The establishment of the RHM complex outside of its 'natural' environment prompted us to investigate whether, in mitotically-dividing cells, this expression regimen was associated with active Mek1, or that Mek1 could be activated under certain conditions. To evaluate Mek1 kinase activity, we monitored the phosphorylation of Threonine 11 on Histone H3 (phospho-Histone H3-T11), a well-characterized substrate of Mek1 during meiotic prophase [82,83]. We initially tested whether expression of Mek1 alone would lead to kinase activation. We compared effects on Histone H3-T11 in cells that contain *pGAL1::GFP-MEK1* or *pGAL1::GST-MEK1*. GST-fusion mediated dimerization of Mek1 leads to (apparently unregulated) Mek1 activation in meiotic cells [28,84].

Likewise, expression of GST-Mek1 in mitotic cells equally lead to a strong increase in phosphorylation of Histone H3-T11, within 4 hours of galactose addition (**Figure 4a**). When probing Mek1 activation, we consistently observed an apparent background level of phospho-Histone H3-T11 in our culture conditions, which might reflect modification of Histone H3-T11 by a kinase pathway activated under certain nutritional conditions [85,86]. Nonetheless, our observation of increased phosphorylation of Histone H3-T11 upon expression of GST-Mek1 suggests that, also in mitotic cells, fusion of GST with Mek1 leads to (uncontrolled) Mek1 kinase activation, likely via forced dimerization. Expression of *GFP-MEK1,* instead of *GST-MEK1*, was not associated with an increase in Histone H3-T11 phosphorylation (**Figure 4d**). Thus, expressing GFP-Mek1 in isolation does not lead to its activity, in contrast to when Mek1 is fused to GST. In meiosis, Mek1 activity is coupled to upstream Mec1/Tel1-dependent phospho-signaling triggered by Spo11-dependent DSB formation [46,47]. A main downstream target of Mec1/Tel1 that enables Mek1 activation is Hop1 [46,47]. Hop1 phosphorylation can be monitored by phospho-specific antibodies or a phosphorylation-induced retardation migration in SDS-PAGE electrophoresis. We queried whether inducing DNA damage in combination with Mek1 expression affected Mek1 activation. We therefore treated cells with methyl methanesulfonate (MMS), a DNA alkylating agent that triggers replication fork stalling and associated DNA damage signaling [87], and monitored Mek1 activation status. Despite the rapid induction of DNA damage (as judged by increased phosphorylation of Serine 129 on Histone H2A (phospho-Histone H2A-S129)), we did not observe an effect on phospho-Histone H3-T11 status (Mek1 activity) in cells expressing *GFP-MEK1* (**Figure 4a**). In cells expressing *GST-MEK1*, MMS treatment did not enhance the apparent activation of Mek1 (**Figure 4a**). Together, these data suggest that, whereas GST-Mek1 shows (apparently unregulated) activation, expression of GFP-Mek1 is not sufficient to trigger downstream phospho-activation, even in the presence of DNA damage induced upstream signaling. We next investigated whether expression of the other RHM complex subunits might accommodate Mek1 activation. The expression of the entire RHM complex did not trigger an increase in Histone H3-Threonine 11 phosphorylation in cells that did not experience DNA damage (**Figure 4b**). Similarly, the induction of DNA damage in cells that did not express the RHM complex, did not lead to an increase in H3-Threonine 11 phosphorylation, despite an increase in Mec1/Tel1-dependent phosphorylation of Histone H2A-S129. Strikingly, when we combined the generation of DNA damage (through MMS treatment) with expression of the RHM complex, we observed a specific phosphorylation of Histone H3-T11 (**Figure 4b**). Thus, in mitotically-dividing cells that expressed the RHM complex and that experienced DNA damage (via MMS treatment), Mek1 kinase became active (**Figure 4b**). MMS is thought to trigger DNA damage signaling via effects on DNA replication [87], which is different from the meiotic DNA damage signaling that occurs during a G2-like state and is triggered by the generation of Spo11-dependent DSBs [88]. Reassuringly, generating DNA damage via phleomycin (a DNA break-inducing agent) treatment also led to Mek1 activation (**Figure 4c**). Thus, when expressed in mitotic cells, the RHM complex can lead to activation of Mek1 kinase,

and that this activation depends on the generation of DNA damage. Querying Mek1 activation in cells expressing different combinations of RHM components (combined with MMS treatment) revealed that Mek1 was only activated when all three RHM complex components were present, as shown in **Figure 4d**. This demonstrates that, as in meiosis, the presence of all three RHM complex subunits is required for efficient Mek1 activation in response to upstream DNA damage signaling. We investigated requirements for upstream Mec1/Tel1-dependent DNA damage signaling. We introduced *mec1Δ* (in a *sml1Δ* background, *i.e., mec1Δ sml1Δ)* and *tel1Δ* into strains expressing the RHM complex, and treated these cells with MMS to induce DNA damage-dependent signaling. Inactivation of *MEC1* led to a marked decrease in phospho-Histone H3-T11 signal, whereas under similar treatment conditions, Tel1 function did not appear to play a significant role in Mek1 activation (**Figure 4e**). These observations are in line with earlier experiments analyzing the regulation of RHM complex activation (via Hop1 phosphorylation) in meiosis [46–49]: also here, Mec1 drives Hop1 phosphorylation (and thus Mek1 activation).

Expressing and activating the RHM complex components in mitosis in principle now allows us to query Mek1 activation mechanisms in ways that are difficult to achieve in meiosis. As a proof-of-principle, we performed two sets of experiments. The first test aimed to address potential cell cycle regulation of Mek1 activation. In meiosis, the RHM complex only becomes active in meiotic G2/prophase, concomitantly with Spo11-dependent DSB formation. Our mitotic activation system allowed us to test if Mek1 could be activated outside of a G2-like cell cycle state. For this, we combined the expression of *RED1*, *HOP1* and *MEK1* with DNA damage induction and cell cycle synchronization in G1 (α-factor treatment) or G2/M (nocodazole treatment). For this experiment, we employed phleomycin as a DNA damaging agent, because MMS is not expected to lead to DNA damage outside of S-phase. Indeed, treatment of MMS in synchronized cells did not lead to detectable activation of Mec1/Tel1-based signaling (*i.e.,* in G1-arrested cultures, **Supplementary Figure 5a**). Cells arrested in G2/M readily activated Mek1, in a manner similar to the activation seen in asynchronously growing cells (**Figure 5a**). However, we found that cells that were arrested in G1 were unable to trigger activation of Mek1, despite the activation of upstream Mec1/Tel1 signaling triggered by phleomycin treatment (**Figure 5a**). These observations suggest that in G1 phase RHM complex activation is inefficient. What could be the reason behind this observation? A possibility is that it is inherent to the RHM complex - *i.e.,* that a crucial modification or event (that normally occurs in meiotic G2/prophase) is lacking in this phase of the mitotic cell cycle, which might preclude RHM complex formation and/or Mek1 activation. We investigated if RHM complex formation was affected in cells that were synchronized in G1 phase of the cell cycle (by α-factor). Co-immunoprecipiation experiments revealed that the RHM complex could be formed efficiently, also in G1-arrested cells (**Figure 5b**), thus likely excluding a failure in RHM complex assembly in G1 phase of the cell cycle. A second possibility is that upstream signaling upon DNA damage induction is lacking or inefficient. Indeed, resection at DNA breaks is limited in G1 phase

[89–91]. Mec1 activity depends on resection, and our data (**Figure 4e**) and earlier work [46–49] suggests that RHM complex activation relies on efficient Mec1 function. Reduced activation of Mec1 – due to diminished DNA end resection in G1 – might thus underlie the failure to activate the RHM complex in G1 phase of mitotic cells.

In addition to being essential in establishing the RHM complex, Red1 and Hop1 also play important roles in establishing the meiotic chromosome loop-axis organization which is key in mediating Spo11 activation [15,19–24]. Indeed, mutations in Red1 and/or Hop1 lead to diminished Spo11-driven DNA break formation in meiosis. Spo11-dependent DNA break formation is required for Mec1/Tel1-dependent Mek1 activation, and any effects on meiotic DNA break activity complicate the interpretation effects of Red1 or Hop1 mutations on Mek1 activation. Our mitotic RHM complex expression and activation system enables us to in principle uncouple the activation of Mek1 from DNA break-dependent signaling. As a second proof-of-principle set of experiments, we therefore used our system to investigate how different truncated Red1 alleles (see earlier and **Figure 2c**) affected Mek1 activation upon DNA damage induction. We expressed the described Red1 truncation alleles – in combination with Hop1 and Mek1 – and monitored the activation of Mek1 upon DNA damage induction (**Figure 5c**). Under these experimental conditions, only the expression of wild type (*i.e.,* full length $Red1_{1-827}$) led to a detectable activation of Mek1 (as judged by phosphorylation of Histone H3-T11). Thus, the integrity of the RHM complex is crucial to enable Mek1 activation. For example, we observed that the presence of COOH region of Red1 is needed for Mek1 activation (**Figure 5c**, $Red1_{1-366}$), despite the fact that this truncated version of Red1 was able to interact with Hop1 as well as Mek1 (**Figure 2d**). Expression of a truncated version of Red1 that expresses the COOH-terminal region of Red1, but lacks its NH_2-terminal ARM/PH domain ($Red1_{346-827}$) was equally not able to activate Mek1. In agreement with the idea that the NH_2-terminal region is however not sufficient for activation was the observation that the removal of the COOH-terminal coiled-coil domain (amino acids 737-827; responsible for tetramerization and filament formation of Red1 [6,15,24] was associated with a lack of Mek1 activation upon expression of this fragment (**Figure 5c**, $Red1_{1-730}$). Hop1 and Mek1 were able to interact with this truncated Red1 protein (**Figure 2d**). In combination with previous work [6,15,24], this suggests that in our mitotic system, tetramerization and/or filament formation of the RHM complex was needed for efficient Mek1 activation. Further truncation revealed that removing the most COOH-terminal 9 amino acids of Red1 (*i.e.,* 819-827) was also associated with a failure in Mek1 activation (**Figure 5c**, $Red1_{1-818}$), whereas this Red1 protein efficiently interacted with Hop1 and Mek1 (**Figure 2d**). Removing this amino acid stretch is associated with defects in meiotic G2/prophase and was suggested to specifically interfere with the filamentous assembly of Red1 (and by interference RHM complexes) [6]. Thus, also in our system, activation of Mek1 (driven by exogenous DNA damage) appears to require filament formation of the RHM complex, an activity that is encoded in the extreme COOH-terminus or Red1 [6,15,24].

We finally evaluated functional consequences of RHMc/Mek1 kinase activation on (mitotic) DNA repair. The current model of RHMc-mediated DNA repair modulation posits that active Mek1 is localized, and as such establishes a localized HR inhibition [60], most prominently mediated through phosphorylation of the Rad51-accessory factor Rad54 [54–59]. Localized inhibition of Rad51-dependent HR could, with the help of additional meiosis-specific events, eventually lead to IH-based repair. The abovementioned growth defect associated with the expression of RHMc (*i.e.,* see **Figure 1f**) precluded us from using these strains to explore effects of RHMc activation on growth in DNA damaging condition. We instead explored effects of activation Mek1 via the expression of the constitutively active GST-Mek1 (**Figure 4a**). As shown in **Figure 6a**, expression of GST-Mek1 (in contrast to the expression of GFP-Mek1) led to a growth defect specifically in cells that experienced DNA damage (either by MMS of phleomycin treatment). The observed effects were similar to effects seen in *rad51Δ* cells (**Figure 6a**), and in mitotic cells that express a Mek1-driven phosphomimetic *RAD54* allele [56]. These findings suggest that activating Mek1 in mitotic cells is sufficient to establish certain characteristics that typify meiosis-specific DNA repair.

Discussion

Here, we report on the establishment of a system enabling controllable expression of a meiosis-specific complex in mitosis. Similar approaches have been used previously to investigate different aspects of meiosis, such as HR repair and chromosome segregation [8–12]. We express components of the trimeric, meiosis-specific Red1, Hop1 and Mek1 complex (*i.e.,* the RHM complex), and show that this complex can self-assemble even when expressed outside of its natural, physiological environment, *i.e.,* in mitotically-dividing cells. This demonstrates that, at least under these conditions, the RHM complex does not require additional meiosis-specific factors or modifications for its assembly. This was somewhat surprising, since earlier work in meiosis has hinted that the incorporation of Mek1 into the Red1-Hop1 complex requires upstream input in the form of Mec1/Tel1-dependent phosphorylation events (most notably on Hop1)[46]. Protein levels and cell cycle status in mitotic versus meiotic conditions might conceivably play a role in causing this apparent difference. We find that the RHM complex can be integrated into mitotic DNA damage-induced kinase signaling, which eventually leads to the activation of Mek1 kinase. Thus, the RHM complex can be formed and activated autonomously in a non-physiological environment.

Our work lays groundwork for further exploration of potential effects of RHM complex activation beyond meiosis on DNA repair dynamics and decisions aimed at testing current models of interhomolog bias establishment (see also below). The initial experiments we describe here provide a proof-of-concept showcasing the feasibility of our experimental approach. We use our system to investigate the requirements for Mek1 activation. We find that all three components of the RHM complex are required for Mek1 activity upon treatment with DNA damaging agents – unless Mek1 is artificially dimerized through GST-fusion, as was also observed in meiotic cells [28,84]. Mitotic activation of the RHM complex in response to DNA damaging conditions relies to a large extent on Mec1 function, mirroring observations made in meiotic cells [46–49]. Furthermore, we found that the activation of Mek1 by upstream Mec1-dependent signaling is impaired in G1-phase of the cell cycle. Mec1 activity is dependent on ssDNA generation at DNA breaks [92,93], and DNA end resection is inefficient in G1 phase due to low Cdk1 activity [89–91]. We suggest that efficient activation of the RHM complex (in mitosis) requires efficient DNA end resection-mediated Mec1 activity.

We probe the dependency of RHM complex formation and activation on Red1 structural domains. Using this approach, we find that although RHM complex formation can be established in several Red1 mutants lacking certain structural and functional domains (**Figure 2d and e**), the activation of Mek1 appears to require full length Red1 protein (**Figure 4c**). We suggest that the highly-controlled assembly and activation of the RHM complex is responsive and reliant on several (upstream) inputs, such as phosphorylation events, chromatin association, filamentous assembly, which eventually leads to the promotion of Mek1 activation. For example, our data indicate that the NH_2-terminal ARM/PH domain of Red1 [61,72,73] is required for the activation of Mek1. It is currently unclear what the molecular role of

this ARM/PH domain is. This domain possibly mediates the association between Red1 and meiotic (Rec8)-containing cohesion [17,32]. Thus, chromosomal association might be key to enabling Mek1 activation and subsequent downstream phosphorylation. Additionally, we show that, while the CM of Red1 is absolutely necessary for interaction with Hop1, the ARM/PH domains also likely interact with the HORMA domain of Hop1 (**Figure 2** and **3**). While the role of this interaction might simply be to enhance the binding affinity, it might also play a role in both the activation of Mek1, or in the recently described enhancement of Hop1 binding to the DSB factor Mer2[7]. Further dissection of this interaction in the context of a larger biochemical reconstitution will be necessary. It will also be key to establish whether the RHM complex is recruited to mitotic chromosomes, and if so, where it is recruited and whether association is dependent on the NH_2-terminal ARML/PH domain of Red1 (and on cohesin). Our structural modeling further suggests that the ARML/PH module might contribute to the efficient interaction between Red1, Hop1 and potentially Mek1 (**Figure 3**, and **Supplementary Figures 3-4**), and this could conceivably also influence Mek1 activation. The modeling we present here suggests that the position of the PH module within the NH_2-terminal region of Red1 might influence Red1-Mek1 association (**Supplementary Figure 3**). A Mek1 interaction 'proficient' constellation of this region might only be achieved under defined (cellular) conditions. We were so far unable to reconstitute a Mek1-Red1-Hop1 complex using in vitro approaches. This might indeed indicate that Mek1-assocation is influenced by additional cellular factors not included in our purified systems. Experimental analysis further suggested that the extreme COOH-terminal region of Red1, including its filament forming domain, is needed to endow the RHM complex with Mek1-activating functionality. In addition to the role of a possible chromatin-interacting domain (in the NH_2-terminus of Red1), the proper assembly of large-scale filaments might enable Mek1 activity, potentially via enhancing (chromatin-associated) substrate availability. Earlier work has shown that filament formation of Red1 is needed for the proper assembly of the meiotic chromosome axis, and for successful meiosis [6,15,74,75]. Higher-order organization of the RHM complex might thus also more directly contribute to efficient activation of Mek1 kinase activity. How this organization contributes to Mek1 activity, and whether it involves facilitating substrate availability or interaction, should be a key future question. Answering this question likely requires combining *in vivo* analysis with *in vitro* biochemical reconstitution of functional RHM complexes.

Expression of Red1, a large protein that can form filamentous assemblies [6,15], is associated with growth defects likely stemming from delayed mitotic progression (**Figure 1f and g**), in agreement with earlier work [71]. Cell cycle delay triggered by Red1 expression is exacerbated under conditions where Hop1, Mek1 or Hop1/Mek1 are co-expressed (**Figure 1f and g**). The nature of these effects in unknown, but it can conceivably be caused by the establishment of large protein assemblies/filaments made up of Red1, and/or Hop1, potentially on mitotic chromosomes. A structure-based mutagenesis analysis with regards to the observed cell cycle effects revealed that indeed the COOH-terminal region of Red1

(responsible for the Red1 multimerization and filament formation [6,15]) was involved and seemed sufficient to trigger cell cycle effects (**Figure 2f**). We note that in addition to driving Red1 filaments, this region was shown to interact with the 9-1-1 DNA damage complex components Mec3 and Ddc2 [74] and SUMO (Smt3) chains [74,75]. Currently, we cannot distinguish whether interaction with any of these factors is associated with the cell cycle arrest we observed, or whether it is indeed a consequence of filament assembly. Further work should be aimed at addressing this question in more detail.

The availability of experimental tools and the characteristics of mitotic cells will allow us to query the role of the RHM complex – and potential sufficiency thereof – in establishing alterations in DNA repair. In mitosis, HR-based repair is primarily executed using repair templates that are present on sister chromatids [14], whereas the RHM complex is crucial in promoting interhomolog-biased repair during meiotic HR-based DSB repair. How the RHM complex – and thus the Mek1 kinase – achieves this sister-to-homolog switch during DBS repair is incompletely understood. Several phospho-substrates of Mek1 have been characterized, and a shared functional consequence of Mek1 function is an inhibitory effect on Rad51-mediated DNA repair [54–57]. Most prominently, Mek1 phosphorylates the Rad51-accessory factor Rad54 [58,59]. This reduces the ability of Rad51 to promote homologous recombination [56,57]. The current model posits that a sister chromatid-restricted Mek1-activity establishes a localized zone on meiotic chromosomes that is not permissive to HR-based DNA repair [60]. Escape from this localized activity – with the goal of allowing DSB repair – could only be achieved by distant repair events, which can be found on homologous chromosomes. As such, local Mek1-driven HR inhibition would essentially encourage homology-based repair through local inhibition of DSB repair. We can now in principle explore this model using our mitotic RHM-activation system. It will allow us to ask a myriad of questions, including but not limited to: *i)* is sister-based HR repair inhibited by RHM complex activation in mitosis? *ii)* Is this associated with reduced Rad51 function, and *iii)* a possible increase in homology-directed repair? *iv)* What are the potential effects of this kind of repair on cell cycle progression and genome stability in mitosis? We here tested the first question, with regards to RHMc function. Expression of GST-Mek1 – a constitutively active Mek1 [28,84] – in mitotic cells leads to sensitivity to DNA damaging conditions, in a manner that is comparable to cells that lack Rad51. These experiments suggest that the activation of Mek1 thus is sufficient to inhibit HR, also in mitotic cells. Hence, these findings are in agreement with the proposed model by which Mek1 can lead to a local inhibition of Rad51-dependent repair [60]. We performed these experiments in haploid cells (*i.e.,* in cells that do not contain homologous chromosomes as alternative repair templates). It will be interesting to explore functional consequences of Mek1 activity in diploid cells, especially in combination with the utilization of directed DNA damage-inducing systems. Several other meiotic factors, such as Rec8 and Hed1, contribute to interhomolog-directed HR bias in meiosis [10,12,56,57,94]. In order to establish a 'more complete' switch to meiosis-like HR repair, it might be required to combine our system with the expression of such factors in mitotically-dividing cells.

The system we describe has the potential to form the basis for innovative experimental approaches aimed at understanding one of the defining features of sexual reproduction: the establishment of a highly specialized HR-based DSB repair pathway. Functional human homologs of RHM components (*e.g.*, HORMAD1/HORMAD2 – Hop1 homologs, and SYCP2/SCYP3 – Red1 homologs) have been described (reviewed in [61,95]), and might act in a comparable fashion during the establishment of interhomolog DNA repair bias, potentially in complex with Chk2. We also note that the human homologs of (non-enzymatic) RHM complex components frequently become aberrantly re-expressed in human cancers, and are proposed to alter DNA repair pathways under pathological conditions (*e.g.*, [96–100]). Our system might provide a conceptual framework to query functionality of human meiosis-specific DNA repair factors and consequences of aberrant expression of these factors on genome maintenance during tumorigenesis.

Acknowledgements

We are grateful to Andrea Musacchio (Max Planck Institute of Molecular Physiology, Dortmund, Germany) for support. We thank Christopher Rath (Max Planck Institute of Molecular Physiology, Dortmund, Germany) for technical support. We thank Franziska Müller and Petra Janning (Max Planck Institute of Molecular Physiology, Dortmund, Germany) for the generation of XL-MS data. We thank Sharvari Tendulkar and Stefan Westermann (University of Duisburg-Essen, Duisburg, Germany) for experimental advice and help. We are grateful to Michael Chang (ERIBA, Groningen, The Netherlands) for sharing yeast strains. We thank members of the Vader lab for insightful discussions and ideas, with special thanks to Richard Cardoso da Silva for scientific input into this project. We thank Maud Schoot Uiterkamp (Amsterdam UMC, Amsterdam, The Netherlands) for comments on the manuscript. This work was made possible with financial support from the Max Planck Society, the European Research Council (ERC-StG URDNA, agreement nr. 638197, to GV), the Amsterdam UMC (Amsterdam UMC Research Fellowship 2020, to GV), and the German Research Foundation (WE 6513/2-1 to JRW).

Conflict of interest

The authors declare no conflict of interest.

Author contributions

VN, LC, SKF and JRW performed experiments and analyzed results. GV, JRW and VN conceptualized the project, and designed experiments. JRW performed *in situ* structural analysis. GV and JRW acquired financial support. GV wrote the manuscript with input from VN and JRW.

Figure legends

Figure 1a

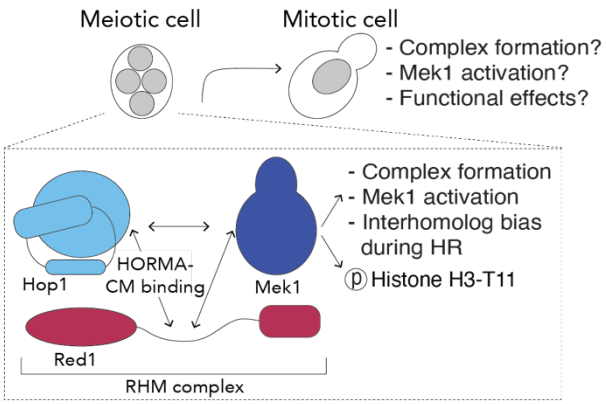

b

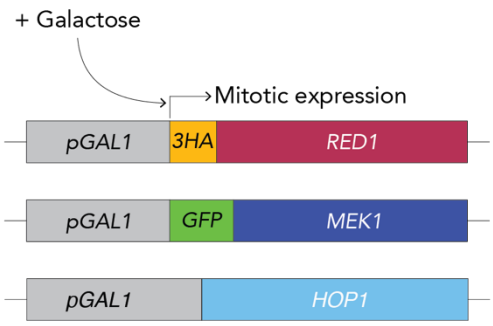

c

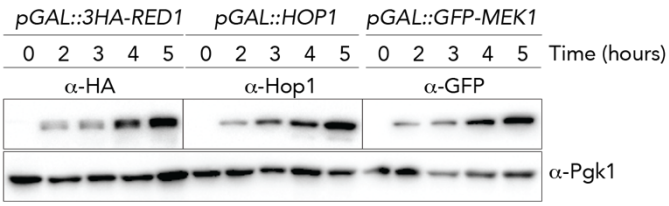

d

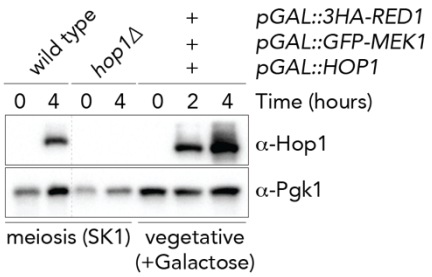

e

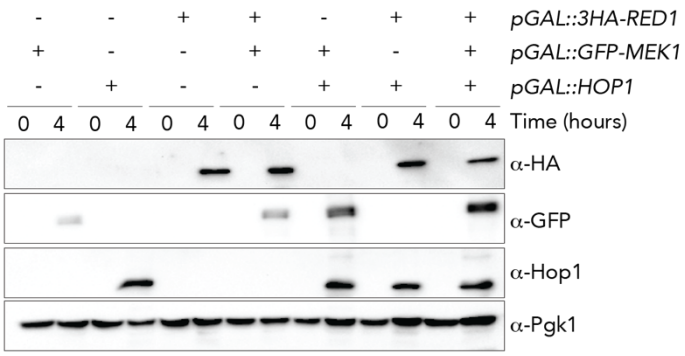

f

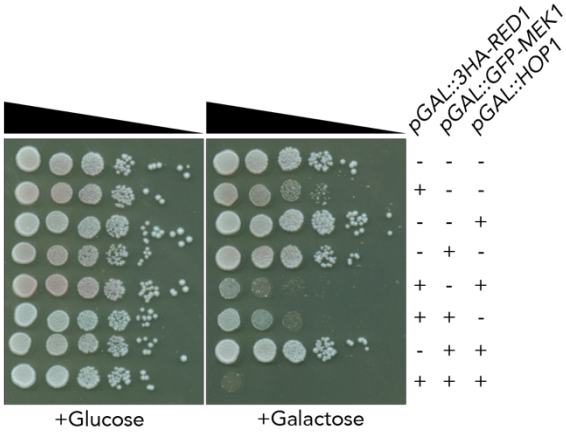

g

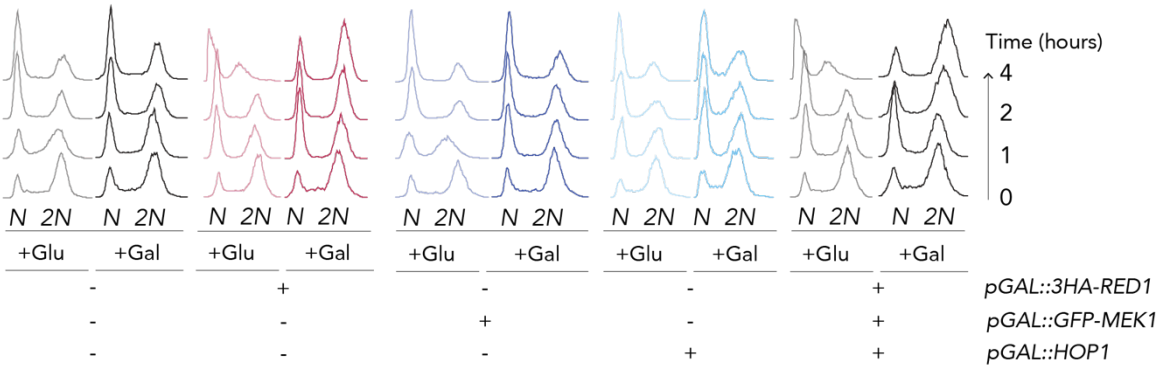

Figure 1. Expression of RHM complex subunits in mitosis.

a. Schematic depicting the Red1-Hop1-Mek1 complex in meiosis, and the conceptual framework of the study. **b**. Schematic of galactose-inducible allele design for *RED1*, *HOP1* and *MEK1*. **c**. Expression analysis of Red1, Hop1, and Mek1 (strains used: yGV3726, yGV3243, and yGV2812). Galactose was added for the indicated time (hours). See also Supplementary Figure 1 for details on growth conditions. α-HA was used to detect Red1, α-GFP was used to detect Mek1, and α-Hop1 was used to detect Hop1. Pgk1 was probed as loading control. **d**. Comparison of Hop1 expression in strains expressing Red1, Mek1 and Hop1 (yGV4806) in mitotic cells (induction time indicated) compared to Hop1 expression in meiotic (SK1) strains (wild type (yGV49) and *hop1Δ* (yGV4442)). In case of mitotic expression, galactose was added for the indicated time (hours). Samples taken at indicated times. α-Hop1 was used to detect Hop1. Pgk1 was probed as loading control. **e**. Expression of Red1, Hop1, and Mek1 in mitotically-dividing cells in strains harboring *pGAL::3HA-RED1*, *pGAL::HOP1*, *pGAL::GFP-MEK1*, and combinations thereof. Strains used are yGV3726, yGV3243, yGV2812, yGV3235, yGV3255, yGV3219, and yGV4806. α-HA was used to detect Red1, α-GFP was used to detect Mek1, and α-Hop1 was used to detect Hop1. Pgk1 was probed as loading control **f**. Serial dilution (10-fold) spotting of yeast strains with indicated genotypes on Glucose- or Galactose-containing solid medium. Strains used are: yGV104, yGV3726, yGV3243, yGV2812, yGV3235, yGV3255, yGV3219, and yGV4806. **g**. Flow cytometry of wild type, *pGAL::3HA-RED1*, *pGAL::HOP1*, *pGAL::GFP-MEK1* and *RED1*, *HOP1* and *MEK1* strains, upon growth in glucose (+Glu) or galactose-containing (+Gal) conditions. Times (hours) indicated. DNA was stained with SYTOX Green. Strains used are: yGV104, yGV3726, yGV3243, yGV2812, and yGV4806.

Figure 2a

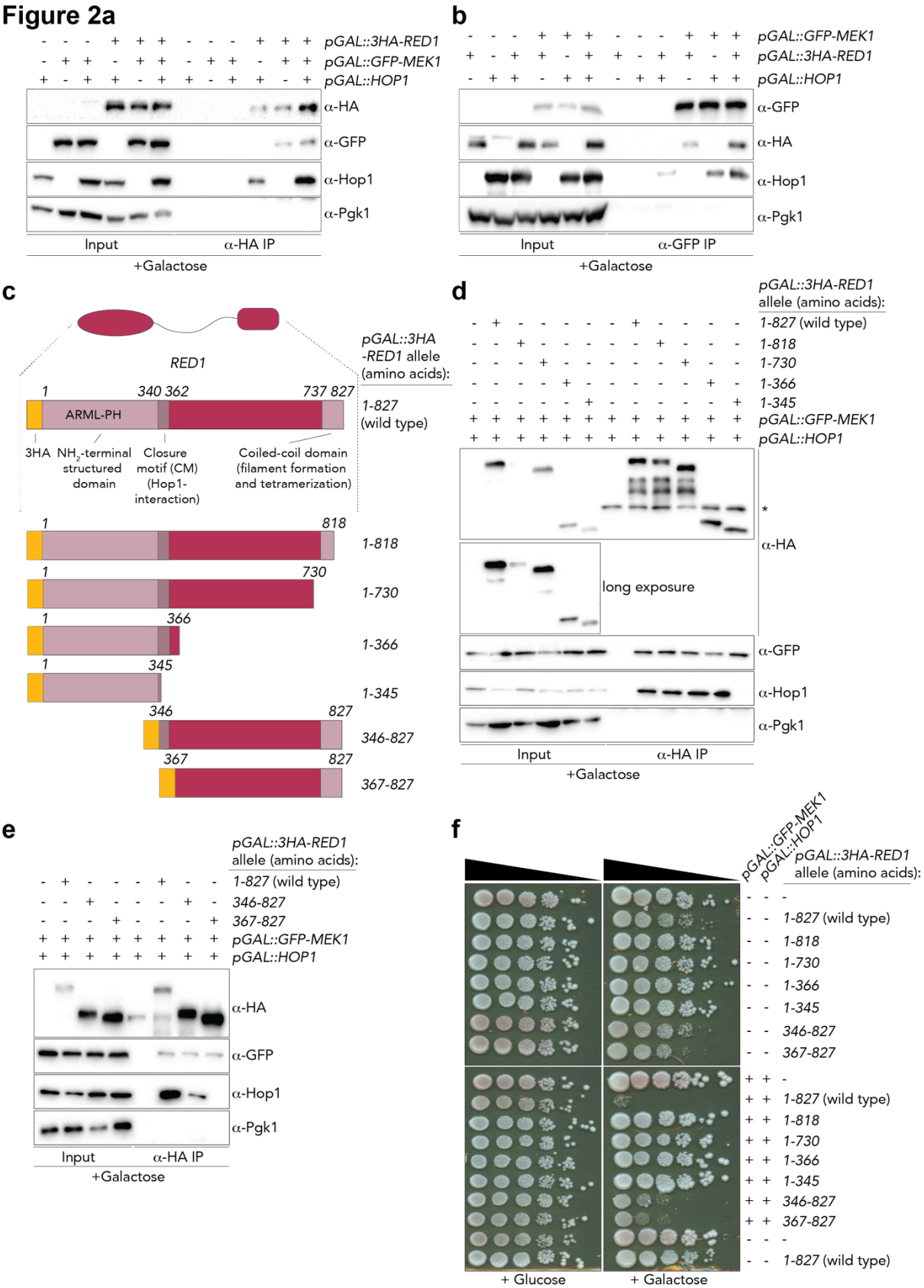
pGAL::3HA-RED1
pGAL::GFP-MEK1
pGAL::HOP1
α-HA
α-GFP
α-Hop1
α-Pgk1
Input
α-HA IP
+Galactose
b
pGAL::GFP-MEK1
pGAL::3HA-RED1
pGAL::HOP1
α-GFP
α-HA
α-Hop1
α-Pgk1
Input
α-GFP IP
+Galactose
c
RED1
pGAL::3HA -RED1 allele (amino acids):
1
340 362
737 827
ARML-PH
3HA
NH2-terminal structured domain
Closure motif (CM) (Hop1-interaction)
Coiled-coil domain (filament formation and tetramerization)
1-827 (wild type)
818
1-818
730
1-730
366
1-366
345
1-345
346
827
346-827
367
367-827
d
pGAL::3HA-RED1 allele (amino acids):
1-827 (wild type)
1-818
1-730
1-366
1-345
pGAL::GFP-MEK1
pGAL::HOP1
*
α-HA
long exposure
α-GFP
α-Hop1
α-Pgk1
Input
α-HA IP
+Galactose
e
pGAL::3HA-RED1 allele (amino acids):
1-827 (wild type)
346-827
367-827
pGAL::GFP-MEK1
pGAL::HOP1
α-HA
α-GFP
α-Hop1
α-Pgk1
Input
α-HA IP
+Galactose
f
pGAL::GFP-MEK1
pGAL::HOP1
pGAL::3HA-RED1 allele (amino acids):
1-827 (wild type)
1-818
1-730
1-366
1-345
346-827
367-827
1-827 (wild type)
1-818
1-730
1-366
1-345
346-827
367-827
1-827 (wild type)
+ Glucose
+ Galactose

Figure 2. Red1-Hop1-Mek1 complex formation in mitosis.

a. Co-immunoprecipitation (co-IP) between Red1, Hop1 and/or Mek1. Red1 was immunoprecipitated via α-HA pulldown. α-HA was used to detect Red1, α-GFP was used to detect Mek1, and α-Hop1 was used to detect Hop1. Pgk1 was probed as loading control. Samples were taken after 4 hours induction with galactose. The following strains were used: yGV3242, yGV2812, yGV3235, yGV3255, yGV3219, yGV4806. **b**. Co-immunoprecipitation (co-IP) between Mek1, Hop1 and/or Red1. Mek1 was immunoprecipitated via α-GFP pulldown. α-HA was used to detect Red1, α-GFP was used to detect Mek1, and α-Hop1 was used to detect Hop1. Pgk1 was probed as loading control. Samples were taken after 4 hours induction with galactose. The following strains were used: yGV3242, yGV3726, yGV3235, yGV3255, yGV3219, yGV4806. **c**. Schematic depicting Red1 structural organization, and Red1 truncation mutants employed in this study. **d**. Co-immunoprecipitation (co-IP) between Red1 (wild type and truncations), and Hop1 and/or Mek1. Red1 was immunoprecipitated via α-HA pulldown. α-HA was used to detect Red1, α-GFP was used to detect Mek1, and α-Hop1 was used to detect Hop1. Pgk1 was probed as loading control. * indicates IgG heavy-chain. Samples were taken after 4 hours induction with galactose. The following strains were used: yGV3219, yGV4806, yGV4393, yGV4395, yGV4397, yGV4400. **e**. Co-immunoprecipitation (co-IP) between Red1 (wild type and truncations), and Hop1 and/or Mek1. Red1 was immunoprecipitated via α-HA pulldown. α-HA was used to detect Red1, α-GFP was used to detect Mek1, and α-Hop1 was used to detect Hop1. Pgk1 was probed as loading control. Samples were taken after 4 hours induction with galactose. The following strains were used: yGV3219, yGV4806, yGV4207, yGV4402. **f**. Serial dilution (10-fold) spotting of yeast strains expressing different Red1 truncations with and without Hop1 and Mek1, on Glucose- or Galactose-containing solid medium. Strains used were: yGV104, yGV3726, yGV3219, yGV3798, yGV3799, yGV4190, yGV4191, yGV4193, yGV4194, yGV4207, yGV4393, yGV4395, yGV4397, yGV4400, yGV4402 and yGV4806.

Figure 3a

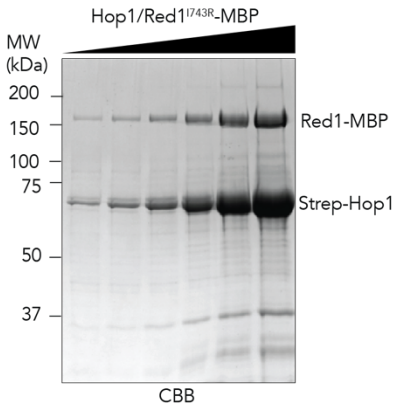

b

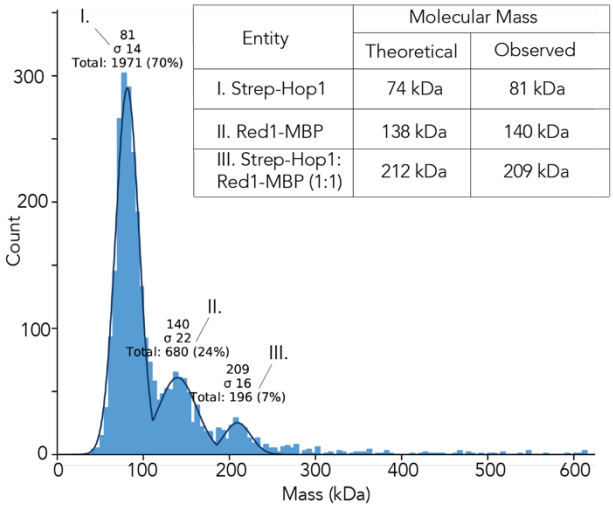

Entity	Molecular Mass	
	Theoretical	Observed
I. Strep-Hop1	74 kDa	81 kDa
II. Red1-MBP	138 kDa	140 kDa
III. Strep-Hop1: Red1-MBP (1:1)	212 kDa	209 kDa

c

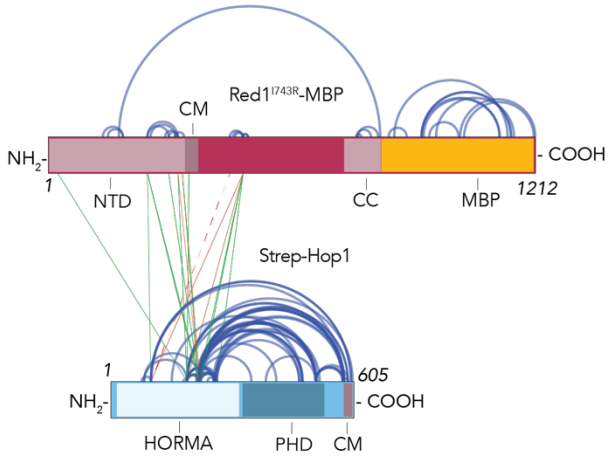

d

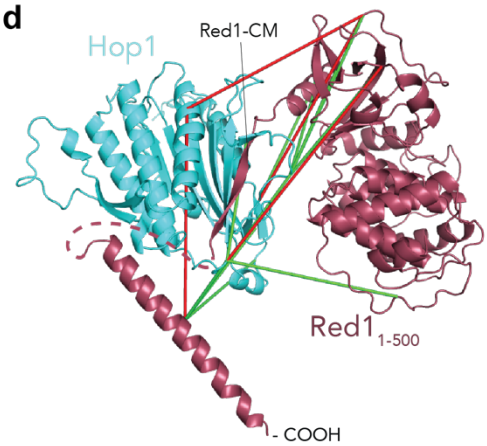

e

Chain 1	Residue	Chain 2	Residue	C_α to C_α distance (Å)	
Hop1	222	Red1	247	42.4	
Hop1	190	Red1	485	17	*
Hop1	264	Red1	485	25.7	*
Hop1	190	Red1	350	24.5	*
Hop1	190	Red1	24	34.7	*
Hop1	219	Red1	334	29.8	*
Hop1	222	Red1	334	33.3	*
Hop1	190	Red1	323	48.4	
Hop1	100	Red1	247	39.5	
Hop1	100	Red1	485	42.1	
Hop1	219	Red1	485	35.8	*
Hop1	219	Red1	300	22.7	*
Hop1	219	Red1	247	34.6	*
Hop1	224	Red1	485	24.8	*
Hop1	219	Red1	323	28.2	*
Hop1	101	Red1	452	62.1	

Figure 3. Purification and analysis of a Hop1-Red1 complex

a. Purity of Hop1-Red1 complex. Increasing quantities of the Strep-Hop1 Red11743R-MBP complex were run on a 10% SDS-PAGE gel. The gel was subsequently stained with coomassie and imaged. **b.** Mass Photometry of Hop1-Red1 complex. Purified Hop1-Red1 complex was diluted to ~30 nM and measured using a Refyen One mass photometer as per the manufacturer's instructions. **c.** XL-MS map of Hop1-Red1. Visualization of the cross-linked Hop1-Red1 complex. Cross-links were filtered for a match score of >100 leading to an FDR of <1%. Intramolecular cross links are shown in blue. Intermolecular cross-links are colored according to whether they are consistent with the model (see main text). The red dotted cross-link is omitted from the model in **d.** for clarity, and is not compatible with the AF2 model. **d**. AlphaFold2 model of Hop1 $Red1_{1\text{-}500}$. $Hop1_{1\text{-}300}$ is colored in blue and oriented to show the HORMA domain. The closure motif of Red1 bound within the HORMA domain is indicated. A long loop in Red1 between residues 361 and 466 has been omitted for clarity and replaced with a dotted line. Cross-links from **c.** were built into the $Hop1_{1\text{-}300}$-$Red1_{1\text{-}500}$ model using PyXlinkViewer [101]. C_α-C_α distances of > 37 Å were considered to be incompatible with the model and are shown as red lines. Distances of <37 Å are shown as green lines. 37Å was chosen as a cutoff based on the maximum C_α-C_α distance for the DSBU cross-linker (27Å)[68] plus the approximate PAE for the model (10Å). **e.** Table showing intersubunit DSBU-crosslink distances derived from the model shown in **d.** * indicates crosslinks that agree with the structural modeling.

Figure 4a

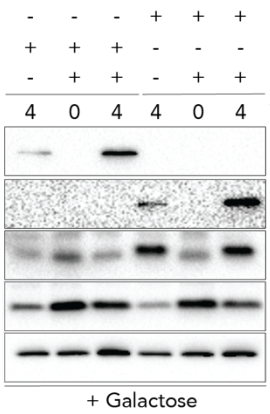

b

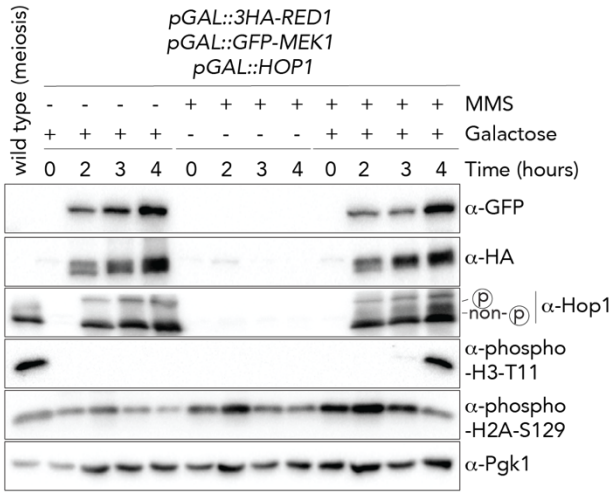

c

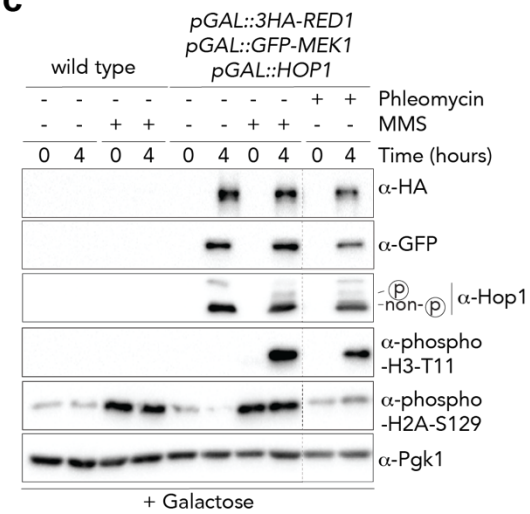

d

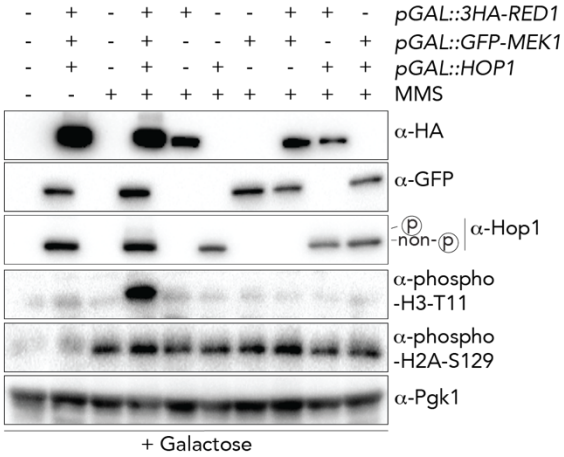

e

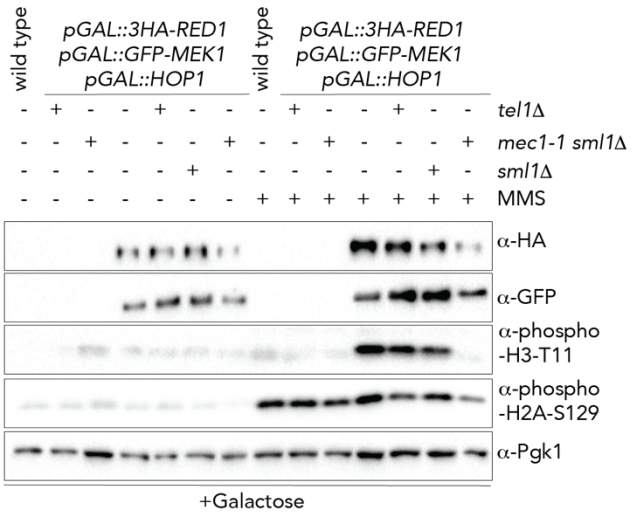

Figure 4. Activation of the RHM complex in mitotically-dividing cells.

a. Analysis of Mek1 activation in mitotically-dividing cells in cells expressing GST-Mek1 (*pGAL::GST-MEK1*; yGV2774) or GFP-Mek1 (*pGAL::GFP-MEK1*; yGV2812). MMS was used to induce DNA damage; cells were treated with MMS for 4.5 hours. 4 hours of galactose-based induction are indicated. See also Supplementary Figure 1 for details on growth and drug treatment conditions. α-phospho-H2A-S129 was used to detect Mec1/Tel1-dependent activation, α-phospho-Histone H3-T11 was used to detect Mek1 activation. α-GST and α-GFP was used to detect Mek1. Pgk1 was probed as loading control. **b**. Analysis of Mek1 activation in cells expressing Red1, Hop1 and Mek1 (yGV4806). MMS was used to induce DNA damage; cells were treated with MMS for 4.5 hours. Hours of galactose-based induction are indicated. α-phospho-H2A-S129 was used to detect Mec1/Tel1-dependent activation, α-phospho-Histone H3-T11 was used to detect Mek1 activation. α-GFP was used to detect Mek1, α-Hop1 was used to detect Hop1 (note also the slower migrating band of Hop1, indicating phosphorylation-mediated gel retardation), and α-HA was used to detect Red1. Pgk1 was probed as loading control. A control sample from meiotic wild type cells (yGV49), 4 hours into the meiotic program was used. **c**. Analysis of Mek1 activation in wild type cells (yGV104) and cells expressing Red1, Hop1 and Mek1 (yGV4806). MMS or Phleomycin was used to generate DNA damage. Hours of galactose-based induction are indicated. α-phospho-H2A-S129 was used to detect Mec1/Tel1-dependent activation, α-phospho-Histone H3-T11 was used to detect Mek1 activation. α-GFP was used to detect Mek1, α-Hop1 was used to detect Hop1 (note also the slower migrating band of Hop1, indicating phosphorylation-mediated gel retardation), and α-HA was used to detect Red1. Pgk1 was probed as loading control. **d**. Analysis of Mek1 activation in cells expressing different combinations of RHM complex subunits (yGV104, yGV3726, yGV3243, yGV2812, yGV3235, yGV3255, yGV3219 and yGV4806). MMS was used to induce DNA damage; cells were treated with MMS for 4.5 hours. Galactose-based induction was done for 4 hours. α-phospho-H2A-S129 was used to detect Mec1/Tel1-dependent activation, α-phospho-Histone H3-T11 was used to detect Mek1 activation. α-GFP was used to detect Mek1, α-Hop1 was used to detect Hop1 (note also the slower migrating band of Hop1, indicating phosphorylation-mediated gel retardation), and α-HA was used to detect Red1. Pgk1 was probed as loading control. **e**. Analysis of Mek1 activation in cells expressing Red1, Hop1 and Mek1 in wild type, *tel1Δ, sml1Δ, and mec1Δ sml1Δ*. MMS was used to induce DNA damage; cells were treated with MMS for 4.5 hours. Galactose-based induction was done for 4 hours. α-phospho-H2A-S129 was used to detect Mec1/Tel1-dependent activation, α-phospho-Histone H3-T11 was used to detect Mek1 activation. α-GFP was used to detect Mek1, α-HA was used to detect Red1. Pgk1 was probed as loading control. Yeast strains used yGV4806, yGV5011, yGV5033, yGV5044.

Figure 5a

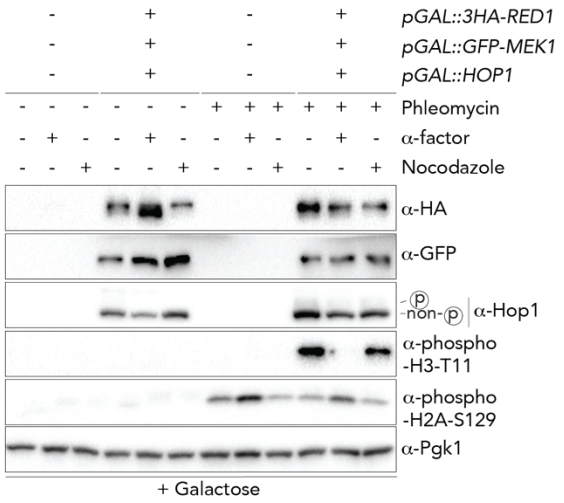
pGAL::3HA-RED1
pGAL::GFP-MEK1
pGAL::HOP1
Phleomycin
α-factor
Nocodazole
α-HA
α-GFP
-ⓟ
-non-ⓟ
α-Hop1
α-phospho
-H3-T11
α-phospho
-H2A-S129
α-Pgk1
+ Galactose

b

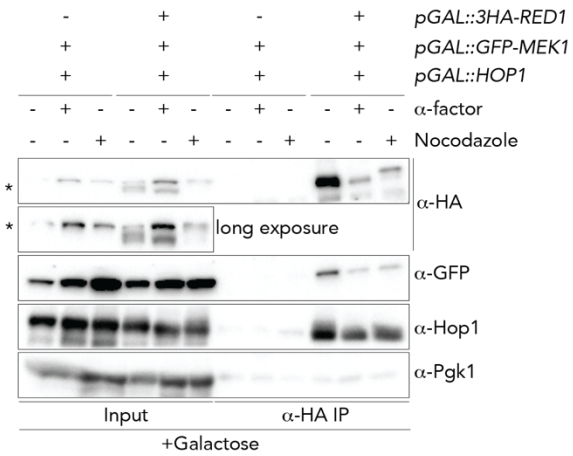
pGAL::3HA-RED1
pGAL::GFP-MEK1
pGAL::HOP1
α-factor
Nocodazole
*
α-HA
long exposure
α-GFP
α-Hop1
α-Pgk1
Input
α-HA IP
+Galactose

c

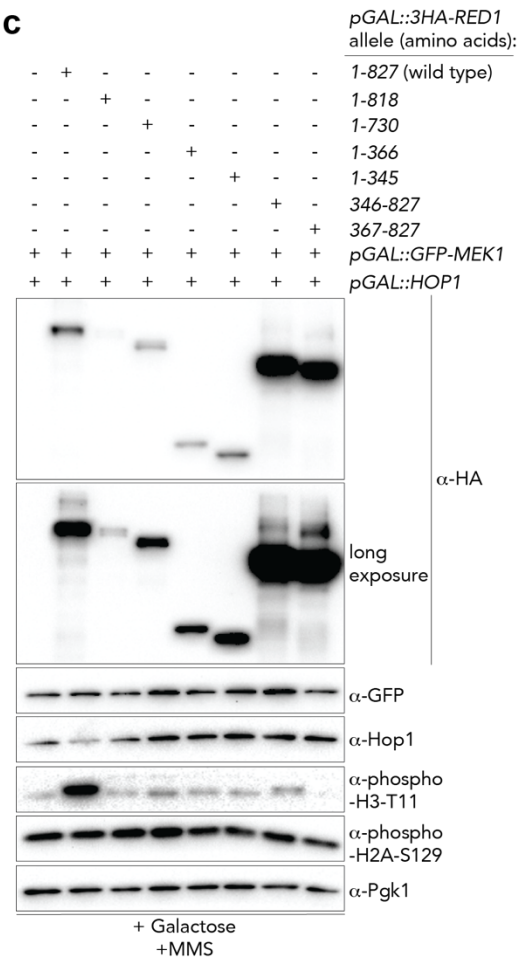
pGAL::3HA-RED1
allele (amino acids):
1-827 (wild type)
1-818
1-730
1-366
1-345
346-827
367-827
pGAL::GFP-MEK1
pGAL::HOP1
α-HA
long
exposure
α-GFP
α-Hop1
α-phospho
-H3-T11
α-phospho
-H2A-S129
α-Pgk1
+ Galactose
+MMS

Figure 5. Analysis of RHM complex assembly and activation during the cell cycle and in the presence of Red1 truncation alleles.

a. Analysis of Mek1 activation in wild type or Red1, Hop1 and Mek1 expressing cells under different cell cycle conditions. Yeast strains used are yG104 and yGV480. Cells were arrested in G1-phase by the addition of α-factor, and in mitosis by addition of nocodazole (see Material and Methods and Supplementary Figure 1 for details). Phleomycin was used to induce DNA damage. Galactose-based induction was for 4 hours. α-phospho-H2A-S129 was used to detect Mec1/Tel1-dependent activation, α-phospho-Histone H3-T11 was used to detect Mek1 activation. α-GFP was used to detect Mek1, α-Hop1 was used to detect Hop1 (note also the slower migrating band of Hop1, indicating phosphorylation-mediated gel retardation), and α-HA was used to detect Red1. Pgk1 was probed as loading control. **c**. Co-immunoprecipitation (co-IP) between Red1 and Hop1/Mek1 under different cell cycle conditions. Cells were arrested in G1-phase by the addition of α-factor, and in mitosis by addition of nocodazole (see Material and Methods for details). Red1 was immunoprecipitated via α-HA pulldown. α-HA was used to detect Red1, α-GFP was used to detect Mek1, and α-Hop1 was used to detect Hop1. Pgk1 was probed as loading control. * indicates background signal. Samples were taken after 4 hours induction with galactose. Yeast strains used: yGV3219 and yGV4806. **c**. Analysis of Mek1 activation in mitotically-dividing cells in cells expressing Hop1 and Mek1, combined with different Red1 truncations. MMS was used to induce DNA damage; cells were treated with MMS for 4.5 hours. Galactose-based induction was for 4 hours. α-phospho-H2A-S129 was used to detect Mec1/Tel1-dependent activation, α-phospho-Histone H3-T11 was used to detect Mek1 activation. α-GFP was used to detect Mek1, α-Hop1 was used to detect Hop1, α-HA was used to detect Red1. Pgk1 was probed as loading control. Strains used were: yGV3219, yGV4806, yGV4393, yGV4395, yGV4397, yGV4400, yGV4207, and yGV4402.

Figure 6a

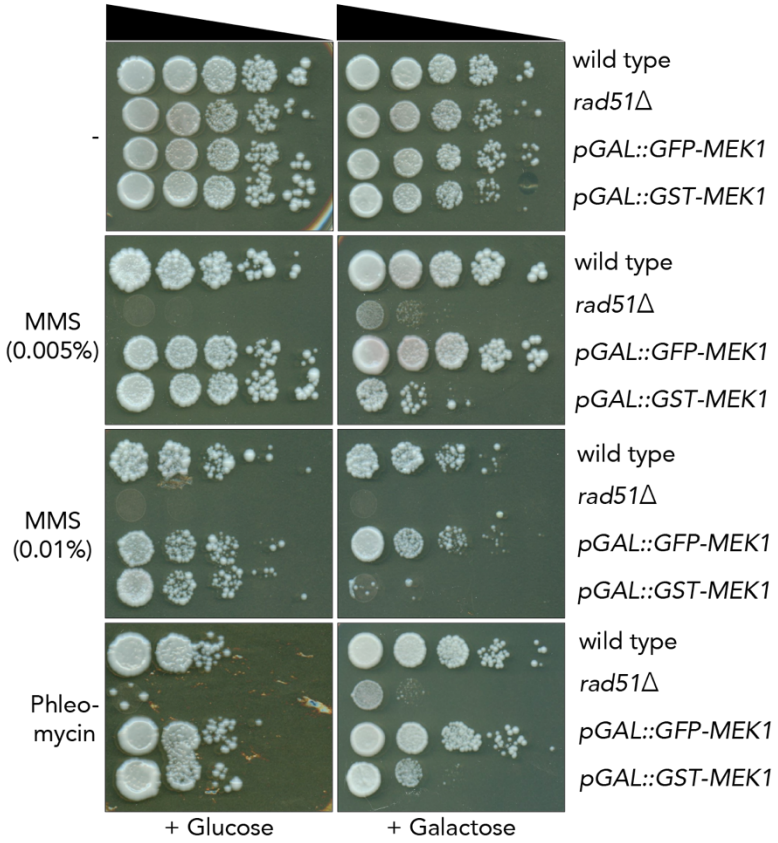

Figure 6. DNA damage sensitivity in cells expressing active Mek1.

a. Serial dilution (10-fold) spotting of yeast strains, on Glucose- or Galactose-containing solid medium, containing MMS (0,005% and 0,01%) or Phleomycin. Strains used were: yGV104, yGV2774, yGV2812, yGV3753.

Supplemental Table 1. Yeast strains.

All strains are of W303 background, except yGV49 and yGV4442 which are of the SK1 background.

Strain number	Genotype
yGV49	*MATa/MATalpha, ho::LYS2, lys2, ura3, leu2::hisG, his4B::LEU2, ARG4/ arg4-Bgl II*
yGV104	*MATa, ade2-1, leu2-3, ura3, trp1-1, his3-11,15, can1-100, GAL, psi+,*
yGV2774	*MATa, ade2-1, leu2-3, ura3, trp1-1, his3-11,15, can1-100, GAL, psi+, mek1:TRP1-PGAL1-GST-MEK1*
yGV2812	*MATa, ade2-1, leu2-3, ura3, trp1-1, his3-11,15, can1-100, GAL, psi+, mek1:TRP1-PGAL1-GFP-MEK1*
yGV3219	*MATa, ade2-1, leu2-3, ura3, trp1-1, his3-11,15, can1-100, GAL, psi+, Hop1::His3MX6-PGAL-HOP1, mek1:TRP1-PGAL1-GFP-MEK1*
yGV3235	*MATa, ade2-1, leu2-3, ura3, trp1-1, his3-11,15, can1-100, GAL, psi+, red1::KANMX6::pGAL-3HA::RED1, hop1::His3MX6-PGAL-HOP1*
yGV3243	*MATa, ade2-1, leu2-3, ura3, trp1-1, his3-11,15, can1-100, GAL, psi+, hop1::His3MX6-PGAL-HOP1*
yGV3255	*MATa, ADE2, leu2-3, ura3, trp1-1, his3-11,15, can1-100, GAL, psi+, red1::KANMX6::pGAL-3HA::RED1, mek1:TRP1-PGAL1-GFP-MEK1*
yGV3605	*MATa, ade2-1, leu2-3, ura3, trp1-1, his3-11,15, can1-100, GAL, psi+, sml1Δ::HphMX6*

yGV3693	*MATa, ade2-1, leu2-3,112, ura3-1, trp1-1, his3-11,15, can1-100,RAD5, mec1Δ::TRP1, sml1Δ::HIS3*
yGV3719	*MATa, ade2-1, leu2-3,112, ura3-1, trp1-1, his3-11,15, can1-100, tel1Δ::URA3*
yGV3726	*MATa, ade2-1, leu2-3,112, ura3-1, trp1-1, his3-11,15, can1-100, red1::KANMX6::pGAL-3HA::RED1*
yGV3753	*MATa, ade2-1, leu2-3,112, ura3-1, trp1-1, his3-11,15, can1-100, rad51Δ::NATMX*
yGV3798	*MATa, ade2-1, leu2-3, ura3, trp1-1, his3-11,15, can1-100, GAL, psi+, red1::KANMX6::pGAL-3HA-345-827-red1*
yGV3799	*MATa, ade2-1, leu2-3, ura3, trp1-1, his3-11,15, can1-100, GAL, psi+, red1::KANMX6::pGAL-3HA-367-827-red1*
yGV4190	*MATa, ade2-1, leu2-3, ura3, trp1-1, his3-11,15, can1-100, GAL, psi+, red1::KANMX6::pGAL-3HA-1-730-red1::TRP1*
yGV4191	*MATa, ade2-1, leu2-3, ura3, trp1-1, his3-11,15, can1-100, GAL, psi+, red1::KANMX6::pGAL-3HA-1-818-red1::TRP1*
yGV4193	*MATa, ade2-1, leu2-3, ura3, trp1-1, his3-11,15, can1-100, GAL, psi+, red1::KANMX6::pGAL-3HA-1-346-red1::TRP1*
yGV4194	*MATa, ade2-1, leu2-3, ura3, trp1-1, his3-11,15, can1-100, GAL, psi+, red1::KANMX6::pGAL-3HA-1-367-red1::TRP1*

yGV4207	*MATalpha, ade2-1, leu2-3, ura3, trp1-1, his3-11,15, can1-100, GAL, psi+, red1::KANMX6::pGAL-3HA-345-827-red1, hop1::His3MX6-PGAL-Hop1, mek1:TRP1-PGAL1-GFP-MEK1*
yGV4393	*MATalpha, ade2-1, leu2-3, ura3, trp1-1, his3-11,15, can1-100, GAL, psi+, hop1::His3MX6-PGAL-Hop1, mek1:TRP1-PGAL1-GFP-MEK1, red1::KANMX6::pGAL-3HA-1-818-red1::TRP1*
yGV4395	*MATalpha, ade2-1, leu2-3, ura3, trp1-1, his3-11,15, can1-100, GAL, psi+, Hop1::His3MX6-PGAL-Hop1, mek1:TRP1-PGAL1-GFP-MEK1, red1::KANMX6::pGAL-3HA-1-367-red1::TRP1*
yGV4397	*MATa, ade2-1, leu2-3, ura3, trp1-1, his3-11,15, can1-100, GAL, psi+, Hop1::His3MX6-PGAL-Hop1, mek1:TRP1-PGAL1-GFP-MEK1, red1::KANMX6::pGAL-3HA-1-346-red1::TRP1*
yGV4400	*MATalpha, ade2-1, leu2-3, ura3, trp1-1, his3-11,15, can1-100, GAL, psi+, Hop1::His3MX6-PGAL-Hop1, mek1:TRP1-PGAL1-GFP-MEK1, red1::KANMX6::pGAL-3HA-1-730-red1::TRP1*
yGV4402	*MATa, ade2-1, leu2-3, ura3, trp1-1, his3-11,15, can1-100, GAL, psi+, hop1::His3MX6-PGAL-Hop1, mek1:TRP1-PGAL1-GFP-MEK1, red1::KANMX6::pGAL-3HA-367-827-red1*
yGV4442	*MATa/ MATalpha, ho::LYS2, lys2, ura3, leu2::hisG, TRP1, his4B::LEU2, MEK1-6HA::KanMX6, hop1::LEU2*
yGV4806	*MATa, ade2-1, leu2-3, ura3, trp1-1, his3-11,15, can1-100, GAL, psi+, red1::KANMX6::pGAL-3HA::RED1, Hop1::His3MX6-PGAL-Hop1, mek1:TRP1-PGAL1-GFP-MEK1*

yGV5011	*MATa, ade2-1, leu2-3,112, ura3-1, trp1-1, his3-11,15, can1-100, GAL, psi+, red1::KANMX6::pGAL-3HA::RED1, Hop1::His3MX6-PGAL-HOP1, mek1:TRP1-PGAL1-GFP-MEK1, tel1Δ ::URA3*
yGV5033	*MATa, ade2-1, leu2-3,112, ura3-1, trp1-1, his3-11,15, can1-100,RAD5, mek1:TRP1-PGAL1-GFP-MEK1, red1::KANMX6::pGAL-3HA::RED1, Hop1::His3MX6-PGAL-HOP1, mec1Δ ::TRP1, sml1Δ ::HIS3*
yGV5044	*MATa, ade2-1, leu2-3, ura3, trp1-1, his3-11,15, can1-100, GAL, psi+, sml1Δ ::HphMX6, red1::KANMX6::pGAL-3HA::RED1, Hop1::His3MX6-PGAL-HOP1, mek1:TRP1-PGAL1-GFP-MEK1*

Supplementary Figure 1

Standard galactose-based induction

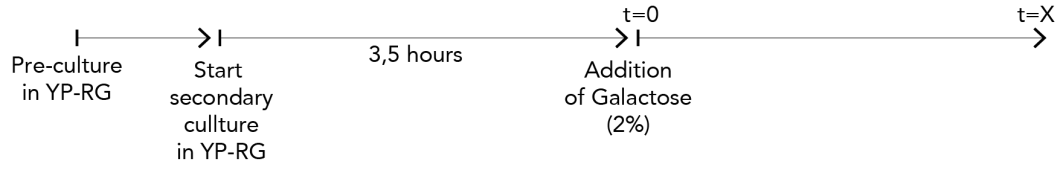

MMS treatment

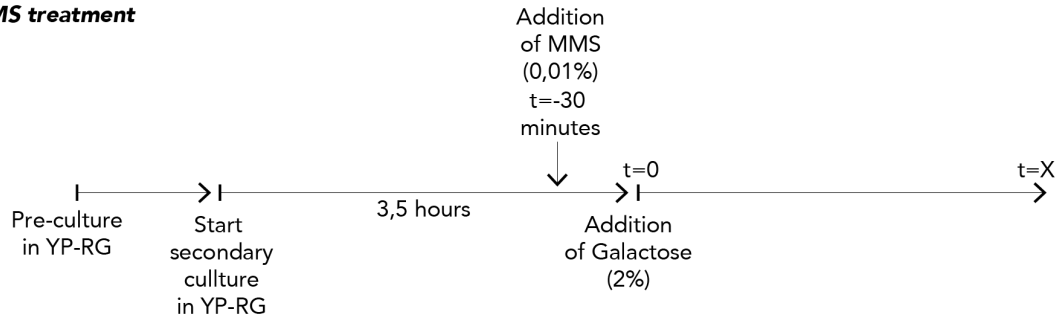

Phleomycin treatment

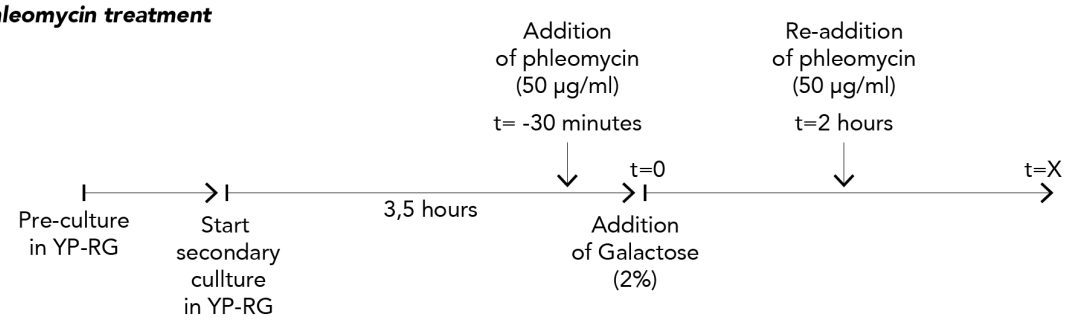

α-factor treatment

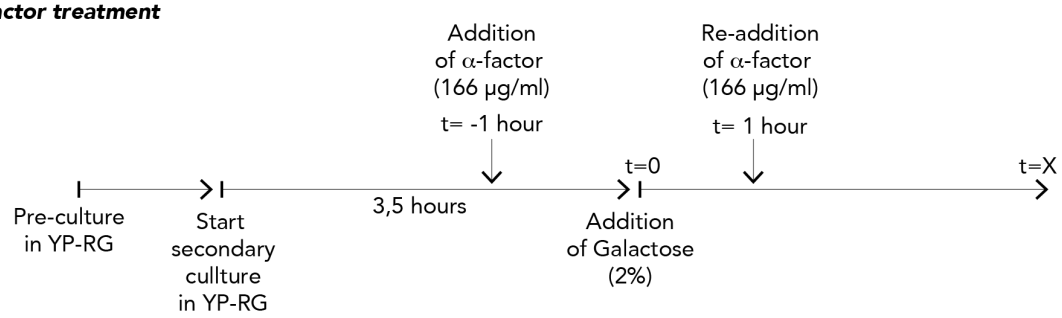

Nocodazole treatment

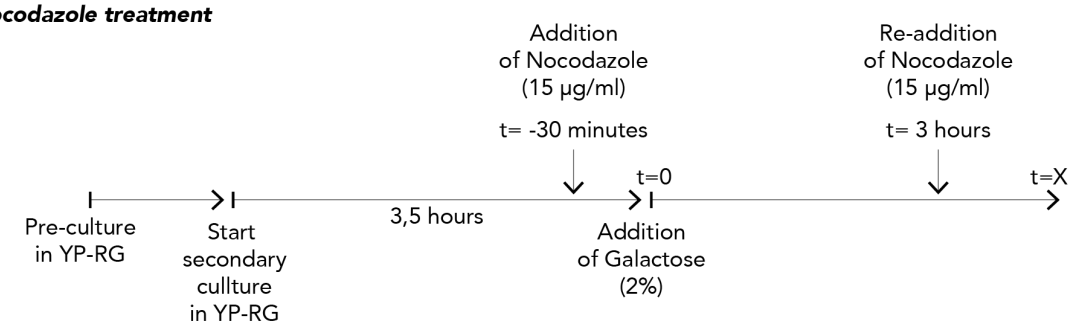

Supplementary Figure 1.

Schematic depicting the different growth and drug treatment regimens used throughout this study. See Material and Methods for more detailed information. Note that in some situations, treatment schemes were combined (such as for example when Phleomycin or MMS treatment was combined with cell cycle synchronization conditions).

Supplementary Figure 2a

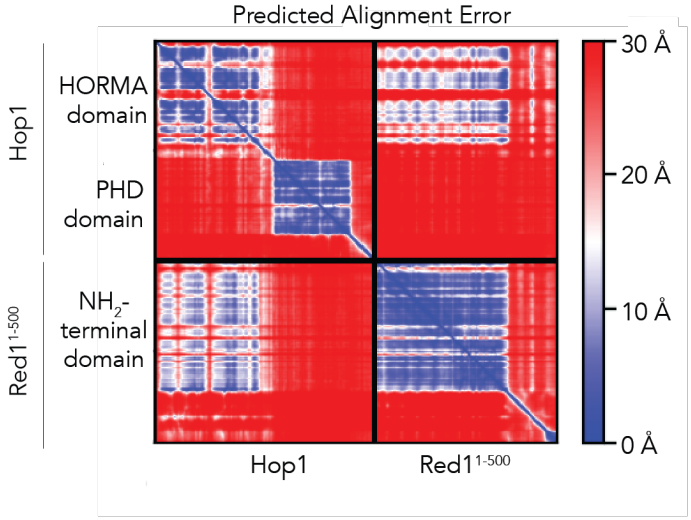

b

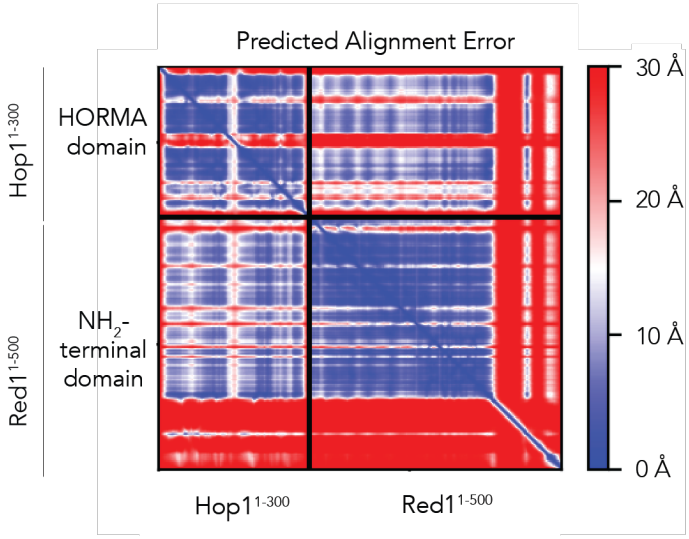

Supplementary Figure 2.

a. Predicted alignment error of the Hop1-Red1$_{1\text{-}500}$ model. The relative position of the Hop1 HORMA domain with the N-terminal domain of Red1 was predicted to be low, consistent with the cross-linking data. The position (though not the fold) of the PHD-like domain of Hop1 is likely to be incorrect. **b.** Predicted alignment error of the Hop1$_{1\text{-}300}$-Red1$_{1\text{-}500}$ model.

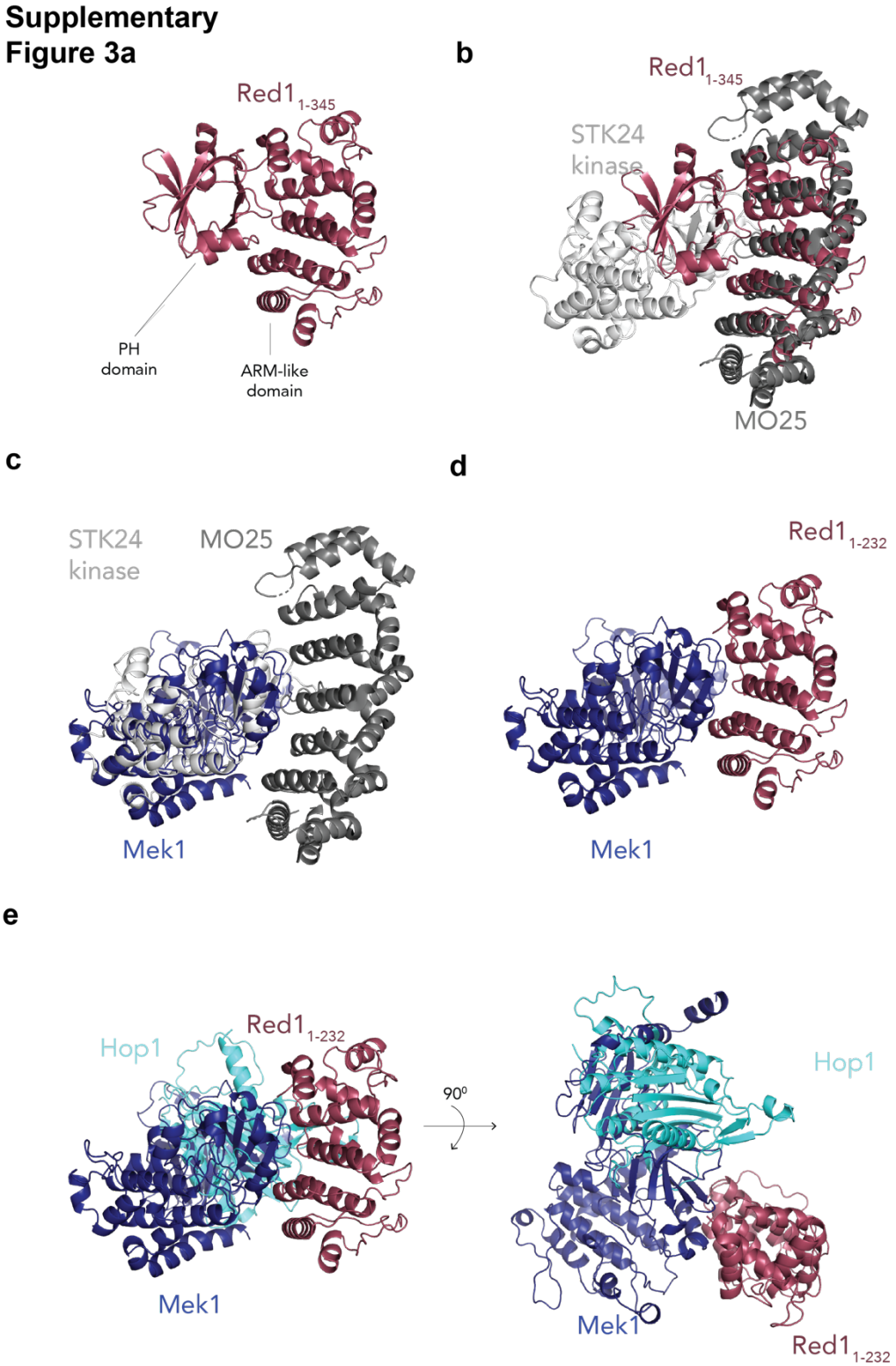

Supplementary Figure 3.

a. Structure prediction of the NH_2-terminal domain of Red1 (amino acids 1-345). The ARML domain (residues 1-226) and the PH domain (residues 227-345) are labelled. **b.** Superposition of the MO25-STK24 crystal structure (3ZHP) on the Red1 ARML domain that was discovered via a DALI search (Z-score 9.6, RMSD 3.0Å over 155 residues). The MO25 is shown in dark grey, the STK24 kinase in light grey. **c.** Matchmaker superposition of the AF2 model of Mek1 onto STK24 kinase (sequence

alignment score = 417.8 RMSD between 130 pruned atom pairs is 1.035 angstroms; (across all 263 pairs: 5.928)) **d.** Combined model from **b**. and **c**., showing Red1 and Mek1. Note that the presence of the PH domain of Red1 in the current orientation is incompatible with the position of Mek1. **e.** Hop1 (as shown **Figure 3)** is included in the assembly and the PH domain of Red1 is removed for clarity. The right panel shows a 90º rotation about the X-axis, revealing the position of the FHA domain of Mek1. In this orientation the FHA domain clashed with Hop1, binding Mek1 with Red1-Hop1 should thus be accommodated by a spatial re-orientation of the FHA domain (potentially upon phospho-peptide binding).

Supplementary Figure 4a

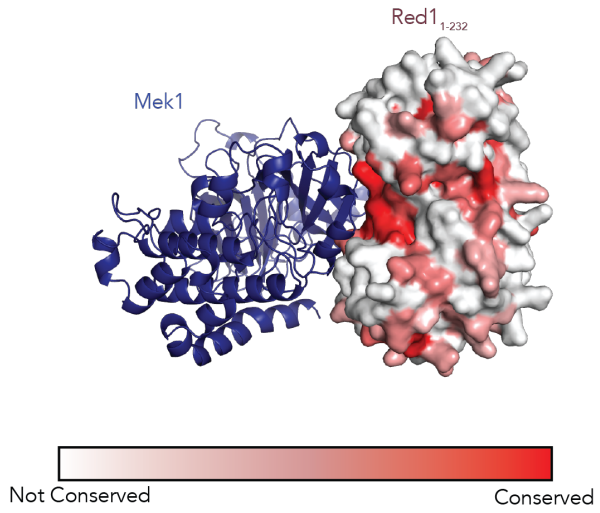

b

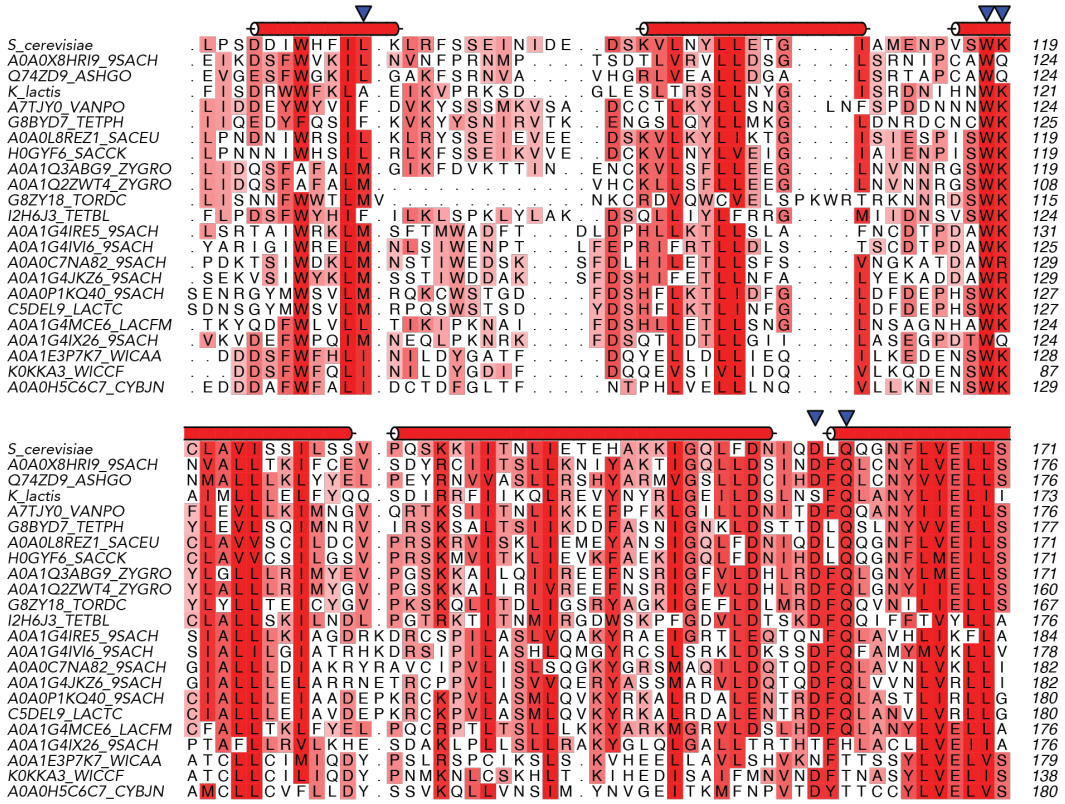

Supplementary Figure 4

a. Previously identified Red1 orthologs from different budding yeasts [73] were aligned using MUSCLE. A subset of these sequences were then used to generate a MSA that was mapped onto the surface of Red1 1-232 using ConSurf [102]. Sequences were coloured in shades of red according to conservation as shown in B). Note the deep red patch that constitutes a hypothetical Mek1 binding site. **b.** Selected

region of Red1 MSA described in **a**. and secondary structure for *S. cerevisiae* sequence based upon the AlphaFold2 model. The putative interaction residues for Mek1 are highlighted with blue arrows.

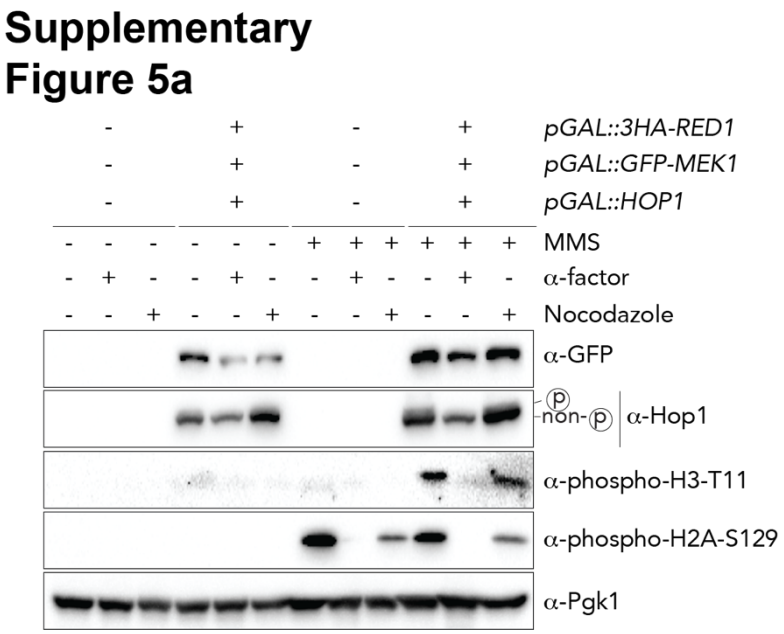

Supplementary Figure 5.

a. Analysis of Mek1 activation in wild type or Red1, Hop1 and Mek1 expressing cells under different cell cycle conditions. Yeast strains used are yGV104 and yGV480. Cells were arrested in G1-phase by the addition of α-factor, and in mitosis by addition of nocodazole (see Material and Methods and Supplementary Figure 1 for details). MMS was used to induce DNA damage. Galactose-based induction was for 4 hours. α-phospho-H2A-S129 was used to detect Mec1/Tel1-dependent activation, α-phospho-Histone H3-T11 was used to detect Mek1 activation. α-GFP was used to detect Mek1, α-Hop1 was used to detect Hop1 (note also the slower migrating band of Hop1, indicating phosphorylation-mediated gel retardation). Pgk1 was probed as loading control.

References

1. Petronczki, M., Siomos, M. F. & Nasmyth, K. Un ménage à quatre: the molecular biology of chromosome segregation in meiosis. *Cell* **112**, 423–440 (2003).
2. Claeys Bouuaert, C. *et al*. Structural and functional characterization of the Spo11 core complex. *Nat. Struct. Mol. Biol*. **28**, 92–102 (2021).
3. Claeys Bouuaert, C. *et al*. DNA-driven condensation assembles the meiotic DNA break machinery. *Nature* **592**, 144–149 (2021).
4. Dunce, J. M., Salmon, L. J. & Davies, O. R. Structural basis of meiotic chromosome synaptic elongation through hierarchical fibrous assembly of SYCE2-TEX12. *Nat. Struct. Mol. Biol*. **28**, 681–693 (2021).
5. Villar-Fernández, M. A. *et al*. Biochemical and functional characterization of a meiosis-specific Pch2/ORC AAA+ assembly. *Life Sci Alliance* **3**, (2020).
6. West, A. M. *et al*. A conserved filamentous assembly underlies the structure of the meiotic chromosome axis. *Elife* **8**, (2019).
7. Rousová, D. *et al*. Novel mechanistic insights into the role of Mer2 as the keystone of meiotic DNA break formation. *Elife* **10**, (2021).
8. Monje-Casas, F., Prabhu, V. R., Lee, B. H., Boselli, M. & Amon, A. Kinetochore orientation during meiosis is controlled by Aurora B and the monopolin complex. *Cell* **128**, 477–490 (2007).
9. Maier, N. K., Ma, J., Lampson, M. A. & Cheeseman, I. M. Separase cleaves the kinetochore protein Meikin at the meiosis I/II transition. *Dev. Cell* **56**, 2192-2206.e8 (2021).
10. Busygina, V. *et al*. Hed1 regulates Rad51-mediated recombination via a novel mechanism. *Genes Dev*. **22**, 786–795 (2008).
11. Varela, E. *et al*. Mitotic expression of Spo13 alters M-phase progression and nucleolar localization of Cdc14 in budding yeast. *Genetics* **185**, 841–854 (2010).
12. Tsubouchi, H. & Roeder, G. S. Budding yeast Hed1 down-regulates the mitotic recombination machinery when meiotic recombination is impaired. *Genes Dev*. **20**, 1766–1775 (2006).
13. Humphryes, N. & Hochwagen, A. A non-sister act: Recombination template choice during meiosis. *Experimental Cell Research* vol. 329 53–60 (2014).
14. Bzymek, M., Thayer, N. H., Oh, S. D., Kleckner, N. & Hunter, N. Double Holliday junctions are intermediates of DNA break repair. *Nature* **464**, 937–941 (2010).
15. Hollingsworth, N. M. & Ponte, L. Genetic interactions between *HOP1, RED1* and *MEK1* suggest that *MEK1* regulates assembly of axial element components during meiosis in the yeast *Saccharomyces cerevisiae*. *Genetics* **147**, 33–42 (1997).
16. Blitzblau, H. G., Chan, C. S., Hochwagen, A. & Bell, S. P. Separation of DNA replication from the assembly of break-competent meiotic chromosomes. *PLoS Genet*. **8**, e1002643 (2012).
17. West, A. M. V., Komives, E. A. & Corbett, K. D. Conformational dynamics of the Hop1 HORMA domain reveal a common mechanism with the spindle checkpoint protein Mad2. *Nucleic Acids Res*. **46**, 279–292 (2018).
18. de los Santos, T. & Hollingsworth, N. M. Red1p, a MEK1-dependent phosphoprotein that physically interacts with Hop1p during meiosis in yeast. *J. Biol. Chem*. (1999).
19. Zickler, D. & Kleckner, N. Meiotic chromosomes: integrating structure and function. *Annu. Rev. Genet*. **33**, 603–754 (1999).
20. Schwacha, A. & Kleckner, N. Interhomolog bias during meiotic recombination: meiotic functions promote a highly differentiated interhomolog-only pathway. *Cell* **90**, 1123–1135 (1997).
21. Mao-Draayer, Y., Galbraith, A. M., Pittman, D. L., Cool, M. & Malone, R. E. Analysis of meiotic recombination pathways in the yeast *Saccharomyces cerevisiae*. *Genetics* **144**, 71–86 (1996).
22. Rockmill, B. & Roeder, G. S. RED1: a yeast gene required for the segregation of chromosomes during the reductional division of meiosis. *Proc. Natl. Acad. Sci. U. S. A*. **85**, 6057–6061 (1988).

23. Blat, Y., Protacio, R. U., Hunter, N. & Kleckner, N. Physical and functional interactions among basic chromosome organizational features govern early steps of meiotic chiasma formation. *Cell* **111**, 791–802 (2002).
24. Woltering, D. *et al*. Meiotic segregation, synapsis, and recombination checkpoint functions require physical interaction between the chromosomal proteins Red1p and Hop1p. *Mol. Cell. Biol*. **20**, 6646–6658 (2000).
25. Hollingsworth, N. M., Goetsch, L. & Byers, B. The *HOP1* gene encodes a meiosis-specific component of yeast chromosomes. *Cell* vol. 61 73–84 (1990).
26. Rosenberg, S. C. & Corbett, K. D. The multifaceted roles of the HORMA domain in cellular signaling. *J. Cell Biol*. **211**, 745–755 (2015).
27. Aravind, L. & Koonin, E. V. The HORMA domain: a common structural denominator in mitotic checkpoints, chromosome synapsis and DNA repair. *Trends Biochem. Sci*. **23**, 284–286 (1998).
28. Niu, H. *et al*. Partner Choice during Meiosis Is Regulated by Hop1-promoted Dimerization of Mek1. *Molecular Biology of the Cell* vol. 16 5804–5818 (2005).
29. Kim, Y. *et al*. The Chromosome Axis Controls Meiotic Events through a Hierarchical Assembly of HORMA Domain Proteins. *Developmental Cell* vol. 31 487–502 (2014).
30. Friedman, D. B., Hollingsworth, N. M. & Byers, B. Insertional mutations in the yeast HOP1 gene: evidence for multimeric assembly in meiosis. *Genetics* **136**, 449–464 (1994).
31. Panizza, S. *et al*. Spo11-accessory proteins link double-strand break sites to the chromosome axis in early meiotic recombination. *Cell* **146**, 372–383 (2011).
32. Sun, X. *et al*. Transcription dynamically patterns the meiotic chromosome-axis interface. *eLife* vol. 4 (2015).
33. Heldrich, J., Markowitz, T. E., Vale-Silva, L. A. & Hochwagen, A. A cohesin-independent mechanism modulates recombination activity along meiotic chromosomes. *bioRxiv* 2020.08.11.247122 (2020) doi:10.1101/2020.08.11.247122.
34. Stanzione, M. *et al*. Meiotic DNA break formation requires the unsynapsed chromosome axis-binding protein IHO1 (CCDC36) in mice. *Nat. Cell Biol*. **18**, 1208–1220 (2016).
35. Kariyazono, R., Oda, A., Yamada, T. & Ohta, K. Conserved HORMA domain-containing protein Hop1 stabilizes interaction between proteins of meiotic DNA break hotspots and chromosome axis. *Nucleic Acids Res*. **47**, 10166–10180 (2019).
36. Panni, S. Phospho-peptide binding domains in *S. cerevisiae* model organism. *Biochimie* **163**, 117–127 (2019).
37. Hollingsworth, N. M. & Gaglione, R. The meiotic-specific Mek1 kinase in budding yeast regulates interhomolog recombination and coordinates meiotic progression with double-strand break repair. *Current Genetics* vol. 65 631–641 (2019).
38. Finn, K., Lowndes, N. F. & Grenon, M. Eukaryotic DNA damage checkpoint activation in response to double-strand breaks. *Cellular and Molecular Life Sciences* vol. 69 1447–1473 (2012).
39. Kar, F. M. & Hochwagen, A. Phospho-Regulation of Meiotic Prophase. *Front Cell Dev Biol* **9**, 667073 (2021).
40. Subramanian, V. V. & Hochwagen, A. The meiotic checkpoint network: step-by-step through meiotic prophase. *Cold Spring Harb. Perspect. Biol*. **6**, a016675 (2014).
41. Vialard, J. E., Gilbert, C. S., Green, C. M. & Lowndes, N. F. The budding yeast Rad9 checkpoint protein is subjected to Mec1/Tel1-dependent hyperphosphorylation and interacts with Rad53 after DNA damage. *EMBO J*. **17**, 5679–5688 (1998).
42. Gilbert, C. S., Green, C. M. & Lowndes, N. F. Budding yeast Rad9 is an ATP-dependent Rad53 activating machine. *Mol. Cell* **8**, 129–136 (2001).
43. Sweeney, F. D. *et al*. *Saccharomyces cerevisiae* Rad9 acts as a Mec1 adaptor to allow Rad53 activation. *Curr. Biol*. **15**, 1364–1375 (2005).
44. Cartagena-Lirola, H., Guerini, I., Manfrini, N., Lucchini, G. & Longhese, M. P. Role of the *Saccharomyces cerevisiae* Rad53 checkpoint kinase in signaling double-strand breaks during the meiotic cell cycle. *Mol. Cell. Biol*. **28**, 4480–4493 (2008).
45. Xu, L., Weiner, B. M. & Kleckner, N. Meiotic cells monitor the status of the interhomolog recombination complex. *Genes Dev*. **11**, 106–118 (1997).

46. Carballo, J. A., Johnson, A. L., Sedgwick, S. G. & Cha, R. S. Phosphorylation of the Axial Element Protein Hop1 by Mec1/Tel1 Ensures Meiotic Interhomolog Recombination. *Cell* vol. 132 758–770 (2008).
47. Penedos, A. *et al*. Essential and Checkpoint Functions of Budding Yeast ATM and ATR during Meiotic Prophase Are Facilitated by Differential Phosphorylation of a Meiotic Adaptor Protein, Hop1. *PLoS One* **10**, e0134297 (2015).
48. Hunter, N. Hop1 and the meiotic DNA-damage response. *Cell* **132**, 731–732 (2008).
49. Schaefer, D., Loidl, J. & Hollingsworth, N. M. Partner choice during meiosis is regulated by Hop1-promoted dimerization of Mek1. *Mol. Biol. Cell* (2005).
50. Suhandynata, R. T., Wan, L., Zhou, H. & Hollingsworth, N. M. Identification of Putative Mek1 Substrates during Meiosis in *Saccharomyces cerevisiae* Using Quantitative Phosphoproteomics. *PLOS ONE* vol. 11 e0155931 (2016).
51. Chen, X. *et al*. Phosphorylation of the Synaptonemal Complex Protein Zip1 Regulates the Crossover/Noncrossover Decision during Yeast Meiosis. *PLoS Biol*. **13**, e1002329 (2015).
52. Lo, H.-C. & Hollingsworth, N. M. Using the semi-synthetic epitope system to identify direct substrates of the meiosis-specific budding yeast kinase, Mek1. *Methods Mol. Biol*. **745**, 135–149 (2011).
53. Prugar, E., Burnett, C., Chen, X. & Hollingsworth, N. M. Coordination of Double Strand Break Repair and Meiotic Progression in Yeast by a Mek1-Ndt80 Negative Feedback Loop. *Genetics* vol. 206 497–512 (2017).
54. Callender, T. L. & Hollingsworth, N. M. Mek1 Suppression of Meiotic Double-Strand Break Repair Is Specific to Sister Chromatids, Chromosome Autonomous and Independent of Rec8 Cohesin Complexes. *Genetics* vol. 185 771–782 (2010).
55. Wan, L., de los Santos, T., Zhang, C., Shokat, K. & Hollingsworth, N. M. Mek1 Kinase Activity Functions Downstream ofRED1in the Regulation of Meiotic Double Strand Break Repair in Budding Yeast. *Molecular Biology of the Cell* vol. 15 11–23 (2004).
56. Niu, H. *et al*. Regulation of meiotic recombination via Mek1-mediated Rad54 phosphorylation. *Mol. Cell* **36**, 393–404 (2009).
57. Callender, T. L. *et al*. Mek1 Down Regulates Rad51 Activity during Yeast Meiosis by Phosphorylation of Hed1. *PLoS Genet*. **12**, e1006226 (2016).
58. Heyer, W.-D., Li, X., Rolfsmeier, M. & Zhang, X.-P. Rad54: the Swiss Army knife of homologous recombination? *Nucleic Acids Res*. **34**, 4115–4125 (2006).
59. Tan, T. L. R., Kanaar, R. & Wyman, C. Rad54, a Jack of all trades in homologous recombination. *DNA Repair* **2**, 787–794 (2003).
60. Subramanian, V. V. *et al*. Chromosome Synapsis Alleviates Mek1-Dependent Suppression of Meiotic DNA Repair. *PLoS Biol*. **14**, e1002369 (2016).
61. Ur, S. N. & Corbett, K. D. Architecture and Dynamics of Meiotic Chromosomes. *Annu. Rev. Genet*. (2021)
62. Bolcun-Filas, E., Rinaldi, V. D., White, M. E. & Schimenti, J. C. Reversal of female infertility by Chk2 ablation reveals the oocyte DNA damage checkpoint pathway. *Science* **343**, 533–536 (2014).
63. Longtine, M. S. *et al*. Additional modules for versatile and economical PCR-based gene deletion and modification in *Saccharomyces cerevisiae*. *Yeast* **14**, 953–961 (1998).
64. Raina, V. B. & Vader, G. Homeostatic Control of Meiotic Prophase Checkpoint Function by Pch2 and Hop1. *Curr. Biol*. **30**, 4413-4424.e5 (2020).
65. Cardoso da Silva, R., Villar-Fernández, M. A. & Vader, G. Active transcription and Orc1 drive chromatin association of the AAA+ ATPase Pch2 during meiotic G2/prophase. *PLoS Genet*. **16**, e1008905 (2020).
66. Altmannova, V., Blaha, A., Astrinidis, S., Reichle, H. & Weir, J. R. InteBac: An integrated bacterial and baculovirus expression vector suite. *Protein Sci*. **30**, 108–114 (2021).
67. Bieniossek, C., Imasaki, T., Takagi, Y. & Berger, I. MultiBac: expanding the research toolbox for multiprotein complexes. *Trends Biochem. Sci*. **37**, 49–57 (2012).
68. Pan, D., Brockmeyer, A., Mueller, F., Musacchio, A. & Bange, T. Simplified Protocol for Cross-linking Mass Spectrometry Using the MS-Cleavable Cross-linker DSBU with Efficient Cross-

link Identification. *Anal. Chem.* **90**, 10990–10999 (2018).
69. Mirdita, M., Ovchinnikov, S. & Steinegger, M. ColabFold - Making protein folding accessible to all. *Bioxriv* (2020).
70. Jumper, J. *et al.* Applying and improving AlphaFold at CASP14. *Proteins* (2021) doi:10.1002/prot.26257.
71. Sopko, R. *et al.* Mapping pathways and phenotypes by systematic gene overexpression. *Mol. Cell* **21**, 319–330 (2006).
72. Feng, J. *et al.* Synaptonemal complex protein 2 (SYCP2) mediates the association of the centromere with the synaptonemal complex. *Protein Cell* **8**, 538–543 (2017).
73. Tromer, E. C., Wemyss, T. A., Ludzia, P., Waller, R. F. & Akiyoshi, B. Repurposing of synaptonemal complex proteins for kinetochores in Kinetoplastida. *Open Biol.* **11**, 210049 (2021).
74. Eichinger, C. S. & Jentsch, S. Synaptonemal complex formation and meiotic checkpoint signaling are linked to the lateral element protein Red1. *Proceedings of the National Academy of Sciences* vol. 107 11370–11375 (2010).
75. Lin, F.-M., Lai, Y.-J., Shen, H.-J., Cheng, Y.-H. & Wang, T.-F. Yeast axial-element protein, Red1, binds SUMO chains to promote meiotic interhomologue recombination and chromosome synapsis. *The EMBO Journal* vol. 29 586–596 (2010).
76. Piano, V. *et al.* CDC20 assists its catalytic incorporation in the mitotic checkpoint complex. *Science* **371**, 67–71 (2021).
77. Dunce, J. M. *et al.* Structural basis of meiotic telomere attachment to the nuclear envelope by MAJIN-TERB2-TERB1. *Nat. Commun.* **9**, 5355 (2018).
78. Holm, L. Using Dali for Protein Structure Comparison. *Methods Mol. Biol.* **2112**, 29–42 (2020).
79. Anuradha, S. & Muniyappa, K. *Saccharomyces cerevisiae* Hop1 zinc finger motif is the minimal region required for its function in vitro. *J. Biol. Chem.* **279**, 28961–28969 (2004).
80. Boekhout, M. *et al.* REC114 Partner ANKRD31 Controls Number, Timing, and Location of Meiotic DNA Breaks. *Mol. Cell* **74**, 1053-1068.e8 (2019).
81. Mehellou, Y. *et al.* Structural insights into the activation of MST3 by MO25. *Biochem. Biophys. Res. Commun.* **431**, 604–609 (2013).
82. Kniewel, R. *et al.* Histone H3 Threonine 11 Phosphorylation Is Catalyzed Directly by the Meiosis-Specific Kinase Mek1 and Provides a Molecular Readout of Mek1 Activity in Vivo. *Genetics* **207**, 1313–1333 (2017).
83. Govin, J. *et al.* Systematic screen reveals new functional dynamics of histones H3 and H4 during gametogenesis. *Genes Dev.* **24**, 1772–1786 (2010).
84. Wu, H.-Y., Ho, H.-C. & Burgess, S. M. Mek1 kinase governs outcomes of meiotic recombination and the checkpoint response. *Curr. Biol.* **20**, 1707–1716 (2010).
85. Oh, S. *et al.* Yeast Nuak1 phosphorylates histone H3 threonine 11 in low glucose stress by the cooperation of AMPK and CK2 signaling. *Elife* **9**, (2020).
86. Oh, S., Suganuma, T., Gogol, M. M. & Workman, J. L. Histone H3 threonine 11 phosphorylation by Sch9 and CK2 regulates chronological lifespan by controlling the nutritional stress response. *Elife* **7**, (2018).
87. Lundin, C. *et al.* Methyl methanesulfonate (MMS) produces heat-labile DNA damage but no detectable in vivo DNA double-strand breaks. *Nucleic Acids Res.* **33**, 3799–3811 (2005).
88. Lam, I. & Keeney, S. Mechanism and regulation of meiotic recombination initiation. *Cold Spring Harb. Perspect. Biol.* **7**, a016634 (2014).
89. Aylon, Y., Liefshitz, B. & Kupiec, M. The CDK regulates repair of double-strand breaks by homologous recombination during the cell cycle. *EMBO J.* **23**, 4868–4875 (2004).
90. Ira, G. *et al.* DNA end resection, homologous recombination and DNA damage checkpoint activation require CDK1. *Nature* vol. 431 1011–1017 (2004).
91. Ferretti, L. P., Lafranchi, L. & Sartori, A. A. Controlling DNA-end resection: a new task for CDKs. *Front. Genet.* **4**, 99 (2013).
92. Ma, M., Rodriguez, A. & Sugimoto, K. Activation of ATR-related protein kinase upon DNA damage recognition. *Curr. Genet.* **66**, 327–333 (2020).
93. Zou, L. & Elledge, S. J. Sensing DNA damage through ATRIP recognition of RPA-ssDNA

complexes. *Science* **300**, 1542–1548 (2003).
94. Kim, K. P. *et al*. Sister cohesion and structural axis components mediate homolog bias of meiotic recombination. *Cell* **143**, 924–937 (2010).
95. Gu, Y., Desai, A. & Corbett, K. D. Evolutionary dynamics and molecular mechanisms of HORMA domain protein signaling. *Annu. Rev. Biochem.* **91**, (2022).
96. Zong, B. *et al*. HORMAD1 promotes docetaxel resistance in triple negative breast cancer by enhancing DNA damage tolerance. *Oncol. Rep.* **46**, (2021).
97. Gao, Y. *et al*. The Cancer/Testes (CT) Antigen HORMAD1 promotes Homologous Recombinational DNA Repair and Radioresistance in Lung adenocarcinoma cells. *Sci. Rep.* **8**, 15304 (2018).
98. Liu, M. *et al*. HORMAD2/CT46.2, a novel cancer/testis gene, is ectopically expressed in lung cancer tissues. *Mol. Hum. Reprod.* **18**, 599–604 (2012).
99. Hosoya, N. & Miyagawa, K. Synaptonemal complex proteins modulate the level of genome integrity in cancers. *Cancer Sci.* **112**, 989–996 (2021).
100. Watkins, J. *et al*. Genomic complexity profiling reveals that HORMAD1 Overexpression contributes to homologous recombination deficiency in triple-negative breast cancers. *Cancer Discov.* **5**, 488–505 (2015).
101. Schiffrin, B., Radford, S. E., Brockwell, D. J. & Calabrese, A. N. PyXlinkViewer: A flexible tool for visualization of protein chemical crosslinking data within the PyMOL molecular graphics system. *Protein Sci.* **29**, 1851–1857 (2020).
102. Ashkenazy, H. *et al*. ConSurf 2016: an improved methodology to estimate and visualize evolutionary conservation in macromolecules. *Nucleic Acids Res.* **44**, W344-50 (2016).